The emergence of a new source of X-rays from the binary neutron star merger GW170817

A. Hajela[1], R. Margutti[1], J. S. Bright[1], K. D. Alexander[1,*], B. D. Metzger[2,3], V. Nedora[4], A. Kathirgamaraju[5], B. Margalit[5], D. Radice[6,7,8], E. Berger[9], A. MacFadyen[10], D. Giannios[11], R. Chornock[1], I. Heywood[12,13,14], L. Sironi[15], O. Gottlieb[16], D. Coppejans[1], T. Laskar[17], Y. Cendes[9], R. Barniol Duran[18], T. Eftekhari[9], W. Fong[1], A. McDowell[10], M. Nicholl[19], X. Xie[20], J. Zrake[21], S. Bernuzzi[4], F. S. Broekgaarden[9], C. D. Kilpatrick[1], G. Terreran[1], V. A. Villar[22], P. K. Blanchard[1], S. Gomez[9], G. Hosseinzadeh[9], D. J. Matthews[1], and J. C. Rastinejad[1]

[1]*Center for Interdisciplinary Exploration and Research in Astrophysics and Department of Physics and Astronomy, Northwestern University, 2145 Sheridan Road, Evanston, IL 60208-3112, USA*

[2]*Department of Physics, Columbia University, New York, NY 10027, USA*

[3]*Center for Computational Astrophysics, Flatiron Institute, 162 W. 5th Avenue, New York, NY 10011, USA*

[4]*Theoretisch-Physikalisches Institut, Friedrich-SchillerUniversität Jena, 07743, Jena, Germany*

[5]*Astronomy Department and Theoretical Astrophysics Center, University of California, Berkeley, Berkeley, CA 94720, USA*

[6]*Institute for Gravitation and the Cosmos, The Pennsylvania State University, University Park, PA 16802*

[7]*Department of Physics, The Pennsylvania State University, University Park, PA 16802*

[*]NHFP Einstein Fellow

[8]*Department of Astronomy & Astrophysics, The Pennsylvania State University, University Park, PA 16802*

[9]*Center for Astrophysics | Harvard & Smithsonian, 60 Garden St., Cambridge, MA 02138, USA*

[10]*Center for Cosmology and Particle Physics, Physics Department, New York University, New York, NY 10003, USA*

[11]*Department of Physics and Astronomy, Purdue University, West Lafayette, IN 47907, USA*

[12]*Astrophysics, Department of Physics, University of Oxford, Keble Road, Oxford, OX1 3RH, UK*

[13]*Department of Physics and Electronics, Rhodes University, PO Box 94, Makhanda, 6140, South Africa*

[14]*South African Radio Astronomy Observatory, 2 Fir Street, Black River Park, Observatory, Cape Town, 7925, South Africa*

[15]*Department of Astronomy and Columbia Astrophysics Laboratory, Columbia University, 550 West 120th Street New York, NY 10027, USA*

[16]*School of Physics and Astronomy, Tel Aviv University, Tel Aviv 69978, Israel*

[17]*Department of Physics, University of Bath, Claverton Down, Bath BA2 7AY, UK*

[18]*Department of Physics and Astronomy, California State University, Sacramento, 6000 J Street, Sacramento, CA 95819-6041, USA*

[19]*School of Physics and Astronomy, University of Birmingham, Birmingham B15 2TT, UK*

[20]*Mathematical Sciences and STAG Research Centre, University of Southampton, Southampton SO17 1BJ, UK*

[21]*Clemson University, 118 Kinard Laboratory Clemson, SC 29634, USA*

[22]*Columbia Astrophysics Laboratory, Columbia University, 550 W 120th St, New York, NY 10027, USA*

The binary neutron-star (BNS) merger GW170817 is the first celestial object from which both gravitational waves (GWs) and light have been detected,[1] enabling critical insight on the pre-merger (GWs) and post-merger (light) physical properties of these phenomena.[2] For the first $\sim$ 3 years after the merger the detected radio and X-ray radiation has been dominated by emission from a structured relativistic jet initially pointing $\sim 15-25$ degrees away from our line of sight and propagating into a low-density medium.[3–6] Here we report on observational evidence for the emergence of a new X-ray emission component at $\delta t > 900$ days after the merger. The new component has luminosity $L_x \approx 5\times10^{38}\,\mathrm{erg\,s^{-1}}$ at 1234 days, and represents a $\sim 3.5\,\sigma$ – $4.3\,\sigma$ excess compared to the expectations from the off-axis jet model that best fits the multi-wavelength afterglow of GW170817 at earlier times. A lack of detectable radio emission at 3 GHz around the same time suggests a harder broadband spectrum than the jet afterglow. These properties are consistent with synchrotron emission from a mildly relativistic shock generated by the expanding merger ejecta, i.e. a kilonova afterglow.[7] In this context our simulations show that the X-ray excess supports the presence of a high-velocity tail in the merger ejecta, and argues against the prompt collapse of the merger remnant into a black hole. However, radiation from accretion processes on the compact-object remnant represents a viable alternative to the kilonova afterglow. Neither a kilonova afterglow nor accretion-powered emission have been observed before.

Gravitational waves (GWs) from the binary neutron star (BNS) merger GW170817 were

detected on 17 August 2017 at 12:41:04 (UT) by Advanced LIGO and Advanced Virgo.[8] The event was rapidly localized to reside in a nearby galaxy at $40.7\,\mathrm{Mpc}$[9] thanks to the identification of its electromagnetic counterpart across the spectrum (γ-rays to radio).[1] During the first ~ 70 days, the electromagnetic spectrum of GW170817 consisted of a combination of thermal emission partially powered by the radioactive decay of heavy chemical elements freshly synthesized in the merger ejecta (i.e. the "kilonova") and non-thermal synchrotron emission dominating in the X-rays and radio bands. The spectrum and flux evolution of the kilonova emission from GW170817 was in agreement with theoretical predictions,[10] demonstrating that mergers of neutron stars are one of the major sources of heavy elements in our Universe. Modeling of the UV-Optical-NIR thermal emission from the kilonova allowed estimates of the bulk velocities and masses of the slower-moving ejecta powering the kilonova: $v \sim 0.1 - 0.3c$ and total ejecta mass $M_{\rm ej} \sim 0.06\,{\rm M}_\odot$, carrying a kinetic energy of $\approx 10^{51}\,\mathrm{erg}$.[11–18]

In the first ≈ 900 days since merger, the non-thermal spectrum of GW170817 has been dominated by synchrotron emission from an ultra-relativistic structured jet initially pointing $\theta_{\rm obs} \sim 15 - 25$ degrees away from our line of sight.[19–21] Radio-to-X-ray data did not show any evidence for spectral evolution across nine orders of magnitude of frequency for 900 days,[3,5,22] and the emission was well characterized as originating from an optically thin synchrotron source with a power-law spectrum $F_\nu \propto \nu^{-(p-1)/2}$ with best-fitting[22] $p = 2.166 \pm 0.026$, where p is the index of the distribution of relativistic electrons responsible for the emission $dN_{\rm e}/d\gamma_{\rm e} \propto \gamma_{\rm e}^{-p}$, where $\gamma_{\rm e}$ is the electron Lorentz factor. Modeling of the multi-wavelength off-axis jet afterglow emission enabled tight constraints on some of the system and environment parameters (or their

combination): for example, the jet kinetic energy to environment density ratio was constrained[19–21] to $E_{\rm k}/n \approx (1-2)\times 10^{53}\,{\rm erg\,cm^3}$ with a credible density range[3] of $10^{-4}\,{\rm cm^{-3}} \leq n \leq 10^{-2}\,{\rm cm^{-3}}$ and the inferred ultra-relativistic jet opening angle is [19–21] $\theta_{\rm jet} \approx 2-5$ degrees. A robust prediction of the off-axis afterglow model post-peak (i.e. after radiation from the core of the jet enters the observer's line of sight) is that of a universal asymptotic light-curve decay with flux[23] $F_\nu(t) \propto t^{-p}$. For the best-fitting jet-environment parameters of GW170817 no broadband spectral evolution is expected, leading to $F_\nu(\nu,t) \propto \nu^{-(p-1)/2}t^{-p}$ (we call this "universal post jet-break model"). Until $\approx$ 900 days post-merger panchromatic observations of the jet afterglow of GW170817 satisfied these expectations (dark blue solid curve, Figure 2).

We acquired deep observations of GW170817 with the *Chandra X-ray Observatory (CXO)*, the Karl G. Jansky Very Large Array (VLA), and the MeerKAT radio interferometer, spanning the time range $\delta t = 1209 - 1273$ days since merger. We found evidence for bright X-ray emission from GW170817 with a statistical significance of $7.2\,\sigma$ (see Methods). The observed count-rate (Extended Data Table 1) implies a $0.3-10$ keV unabsorbed flux of $\sim 2.5\times10^{-14}\,{\rm erg\,cm^{-2}\,s^{-1}}$ (luminosity of $\sim 5\times10^{38}\,{\rm erg\,s^{-1}}$) at $\delta t = 1234$ days (exposure-time weighted mean epoch of the X-ray observations). Because of the limited count statistics, we assumed a power-law spectrum $F_\nu \propto \nu^{-\beta}$ with $\beta = 0.6$ for the flux calibration, as inferred from previous X-ray observations of GW170817 (see Methods). The measured flux is a factor ≈ 4 larger than the extrapolation of the structured-jet model to the present epoch (Figure 2).

We contrast our data against two theoretical models to quantify the statistical evidence of

an X-ray excess of emission compared to the jet-afterglow model that explains the broadband non-thermal emission from GW170817 at $\delta t \leq 900$ days. First, we used the universal post jet-break model to fit the post-peak multi-wavelength afterglow decay. Second, we used the structured off-axis jet afterglow models as implemented in `JetFit`,[24] which utilizes a "boosted-fireball framework"[25] to dynamically evolve the jet as it spreads. In both cases, we self-consistently accounted for the Poisson nature of the process that regulates the detected X-ray signal and performed our statistical tests in the phase-space of observed *CXO* counts (see Methods). Based on these two methods, we find that the probability of a statistical fluctuation lies in the range $P = 1.7 \times 10^{-5} - 4.7 \times 10^{-4}$. We conclude that CXO observations at $\delta t > 900$ days support the evidence of an excess of X-ray emission compared to the jet afterglow predictions with statistical significance of $3.5\,\sigma - 4.3\,\sigma$ (Gaussian equivalent).

In contrast to the X-rays, we did not find evidence for significant radio emission at the location of GW170817 (Figure 2, lower panel, and Figure 1), and we place $3\,\sigma$ flux density upper limits of 39, 5.1, and 5.1 μJy at mean frequencies of 0.8, 3 and 15 GHz, respectively, with MeerKAT and the VLA ($3 \times$ RMS, see Methods). At 3 GHz, this translates to a luminosity of $\lesssim 10^{25}\,\mathrm{erg\,s^{-1}\,Hz^{-1}}$ ($3\,\sigma$ upper limit). The lack of detectable radio emission at the time of the X-ray excess suggests spectral evolution of the source (Extended Data Figure 4). Assuming that the broadband radio-to-X-ray spectrum at ~ 1234 days still follows a simple power-law that we parameterize as $F_\nu \propto \nu^{-(p-1)/2}$, we computed the probability of obtaining a radio detection given the observed X-ray flux as a function of p. As before, we accounted for deviations from Gaussian statistics that manifest in the regime of low spectral counts (see Methods). We find that values of

$p \geq 2.166$, which is the best-fitting value of the jet-afterglow at $\delta t < 900$ days,[22] are ruled out with a statistical confidence $\geq 92\% - 99.2\%$ (Extended Data Figure 5). These results suggest the evolution of the broadband spectrum towards lower values of p and constitute the first indication of spectral evolution of the non-thermal emission from GW170817. The recently reported radio flux density[26] of GW170817 would only strengthen these conclusions (Extended Data Figure 5).

= Balasubramanian et al.

6 DISCUSSION

A number of factors could in principle lead to a late-time X-ray light-curve flattening. Potential scenarios fall into two major categories: (i) "same-shock" scenarios,[27–31] which include an environment over-density encountered by the blast wave; new energy deposited into the shock; and dynamical effects (i.e., the deceleration of the jet into the sub-relativistic phase and the accompanying emergence of the counter-jet emission). (ii) The emergence of an additional emission component either in the form of a kilonova afterglow[7,32] or radiation powered by accretion onto the newly formed compact object. We discuss each model in detail in Methods. We conclude that each of the "same-shock" scenarios would require an ad hoc evolution of key physical parameters of the system to be consistent with the observed phenomenology and are thus disfavored.

7 PREFERRED SCENARIO → Kilonova Afterglow

The deceleration of the fastest tail of the kilonova ejecta into the merger environment (also called "kilonova afterglow") instead represents a natural source of energy to power synchrotron radiation across the electromagnetic spectrum on timescales of $\sim$ years after the BNS merger.[7] In close similarity to stellar explosions, the thermal UV-optical-IR emission traces the slower moving kilonova ejecta ($v \sim 0.1 - 0.3\,c$; Figure 3, upper panel) to which the bulk of the kinetic energy is coupled, while non-thermal emission is a tracer of the fastest ejecta in the outflow ($v \gtrsim 0.4\,c$).

The emergence of this kilonova afterglow, which originates from a quasi-spherical shock that is different from the jet afterglow shock, can naturally explain the observed broadband spectral evolution of the radiation, as the value of p may be different in the two shocks. The theory of Fermi acceleration in the test particle limit[33–35] predicts a value $p < 2.2$ for mildly relativistic shocks, such as that produced by the kilonova, consistent with the observed broadband spectral hardening.

The luminosity and time evolution of the kilonova afterglow from a BNS merger depends on a combination of intrinsic and extrinsic parameters.[7,32] Intrinsic parameters include how the ejecta energy is partitioned in the velocity space $E_{\rm KN}(\Gamma\beta)$, which ultimately depends on the neutron star equation of state (EoS) and the binary mass ratio q. Extrinsic parameters include those that regulate the kilonova shock microphysics (fraction of post-shock energy density in relativistic electrons, $\epsilon_{\rm e,KN}$, and in magnetic field, $\epsilon_{\rm B,KN}$ and $p_{\rm KN}$), and the environment density n. The kilonova afterglow can be used to map the properties of the high-velocity tail of the kilonova ejecta, which is not constrained by the modeling of the early-time UV/optical/NIR emission. We explore different kilonova ejecta profiles as follows. First, we parameterize the kinetic energy distribution as a power-law in specific momentum $\Gamma\beta$: $E_{\rm KN} \propto (\Gamma\beta)^{-\alpha}$ above some minimum specific momentum $\Gamma_0\beta_0$. Motivated by the results from the modeling of the thermal kilonova,[11–18] we adopted a "total" kilonova kinetic energy $E_{\rm KN}(\Gamma_0\beta_0) = 10^{51}\,{\rm erg}$ (Figure 3). This analytical model captures all types of kilonova ejecta, including the dynamical ejecta as well as the disk winds which might have dominated the mass of the kilonova. We explored the multi-dimensional parameter space of intrinsic and extrinsic parameters (Extended Data Figure 6) and generated a set of multi-wavelength kilonova afterglow light-curves adopting $p_{\rm KN} = 2.05$ (consistent with the broadband

SED of Extended Data Figure 4) and $\epsilon_{\rm e,KN} = 0.1$. In Figure 2 we show a set of X-ray and radio kilonova afterglow light-curves for our fiducial set of parameters $\beta_0 = 0.35$, $n = 10^{-3}\,{\rm cm}^{-3}$ and $\epsilon_B = 10^{-3}$ for a range of ejecta stratification parameter values $\alpha = [2, 9]$. Ejecta profiles with $\alpha = 4-6$ can reasonably account for observations at $\delta t > 900$ day. However, the parameter space is currently highly degenerate (Extended Data Figure 6).

As a refinement to the previous model, and to further demonstrate the effect of the intrinsic parameters of the NS binary on the observed kilonova afterglow light-curves, we computed the synchrotron emission (Nedora et al. in prep) from more realistic ejecta profiles obtained from ab-initio numerical relativity BNS merger simulations performed with the `WhiskyTHC`[36–38] code. In these simulations the kilonova ejecta are of dynamical nature and do not include the contribution of disk winds. Figure 3 shows the resulting kinetic energy profiles and mass distribution of a set of simulations that can successfully reproduce the detected X-ray emission in GW170817 for some combination of extrinsic parameters (Extended Data Figure 8). The NS EoS and the binary mass ratio q leave clear imprints on the mass and kinetic energy distribution of the high-velocity tail of the kilonova ejecta. While a variety of NS EoS and binary mass ratios can accommodate our observations, a common ingredient of successful models is binaries that do *not* undergo prompt black hole (BH) collapse. This is a consequence of the fact that in these simulations a post-merger bounce is necessary to launch sufficiently fast and massive kilonova outflows.

In addition to the nature of the compact-object remnant, the early detection of a kilonova afterglow a few years after the merger and its future modeling can enable fundamental insight into

two other still-open questions pertaining to GW170817: the presence of a free-neutron component of ejecta, and the origin of the detected prompt γ-rays.[39,40] Fast ejecta with mass $\gtrsim 10^{-4}\,\mathrm{M}_\odot$ at velocity $v \geq 0.5$c (light-blue shaded area in Figure 3, lower panel) are expected to lead to a freeze out of the r-process,[41] as most neutrons will avoid capture, leaving behind free neutrons that can power a short-lived (i.e. $\approx$hrs) but luminous UV/optical transient. Additionally, kilonova ejecta profiles extending to velocities $v \geq 0.6\,c$ (light-green shaded area in Figure 3, lower panel) provide the necessary conditions to produce γ-rays from a shock breakout of a wide-angle outflow (i.e. the cocoon) inflated by the jet from the merger ejecta.[42,43] Being sensitive to the presence and properties of the fast kilonova ejecta, the kilonova afterglow is thus a probe of the merger dynamics and nature of the compact object remnant.

Radiation powered by an energy release associated with the compact-object remnant either in the form of accretion (for a BH remnant) or spin-down energy (for a long-lived NS remnant), offers an alternative explanation to the presence of an X-ray excess that is not accompanied by bright radio emission. Theoretical arguments based on the presence of a relativistic jet and the overall energetics and colors of the thermal kilonova argue in favor of a hypermassive NS that collapsed to a BH within ≈ 1 s after the merger,[44–51] and the detected X-ray luminosity $L_x \sim 5 \times 10^{38}\,\mathrm{erg\,s^{-1}}$, which is $\approx L_{\rm Edd}$ for a compact-object with mass of a few $\mathrm{M}_\odot$, is highly suggestive of accretion processes at work. A long-lived NS cannot be entirely ruled out, but it is an unlikely scenario based on the exceedingly low magnetic field $B \approx 10^9$ G necessary to match the observed X-ray luminosity ($L_{\rm sd} \simeq 7 \times 10^{38}\,\mathrm{erg\,s^{-1}}\left(\frac{B}{10^9\,\mathrm{G}}\right)^2\left(\frac{P_0}{0.7\,\mathrm{ms}}\right)^{-4}$).

Extended Data Figure 9 shows the evolution of the accretion-powered fall-back X-ray luminosity on a BH remnant, both intrinsic (orange solid line) and observed (red dashed line), i.e. with a correction for absorption by the kilonova ejecta of the form $\propto (1 - e^{-(t/t_{\rm thin})^2})$, where $t_{\rm thin} \approx 1000$ days, when the ejecta becomes optically thin. We compare the properties of the new emission component of GW170817 with known properties of stellar-mass compact-objects accreting close to or above the Eddington rate, i.e. X-ray binaries (XRBs) in the "soft" state and ultra-luminous X-ray (ULXs) sources. The X-ray spectra of these binaries are well modeled by a thermal disk with effective temperature $kT_{\rm eff} \simeq 2\,{\rm keV}\left(\frac{f_{\rm b}}{0.1}\right)^{1/4}\left(\frac{L_{\rm X}}{5\times10^{38}{\rm erg\,s^{-1}}}\right)^{1/4}\left(\frac{M_\bullet}{2.5M_\odot}\right)^{-1/2}$, where f_b is the beaming fraction and $M_\bullet$ is the mass of the compact-object remnant, while having no associated persistent radio emission.[52,53] Similarly, a radio survey of ULXs,[54] which harbor compact objects accreting with luminosity $\geq L_{\rm Edd}$, revealed that their persistent radio emission is suppressed to $\sim 10^{24}\,{\rm erg\,s^{-1}\,Hz^{-1}}$, consistent with the observations of GW170817. Differently from the kilonova afterglow, where the radio emission is expected to brighten with time (Figure 2), this accretion model predicts a constant or declining X-ray emission *without* accompanying bright radio emission.

Observations of GW170817 are mapping an uncharted territory of the BNS merger phenomenology and have far-reaching theoretical implications. Measuring the time of peak of the kilonova afterglow, which probed the ejecta dynamics independent of shock microphysics, would offer a unique opportunity to do calorimetry of the kilonova's fastest ejecta. Alternatively, the detection of a constant (or declining) source of X-ray emission in the next thousands of days that is not accompanied by bright radio emission will unveil how accretion processes work on a compact-

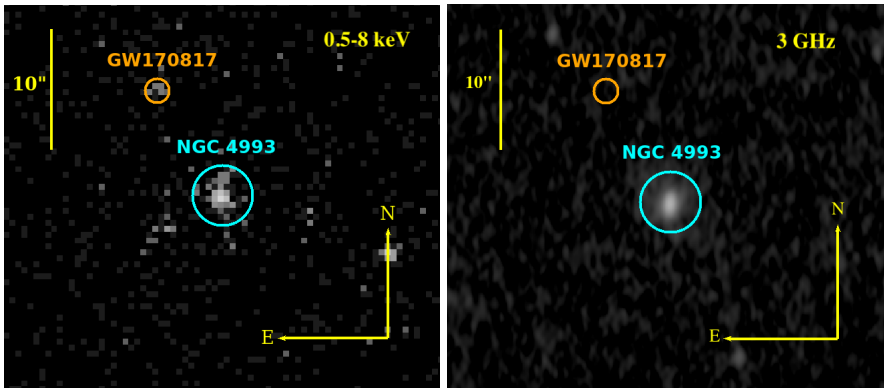

Figure 1 | Combined images of GW170817 at δt ~ 3.4 years: *Left Panel*: Combined X-ray image consisting of *CXO* observations spanning $\delta t \sim 1209 - 1258$ days in the 0.5 – 8 keV energy range. An X-ray source is clearly detected at the location of GW170817 with statistical significance of $7.2\,\sigma$ (Extended Data Table 1). *Right Panel*: Combined radio image comprising VLA 3 GHz observations acquired in the time range $\delta t \sim 1216 - 1265$ days. No radio emission is detected at the location of GW170817. The RMS noise around the location of the BNS merger is $\sim 1.7\,\mu$Jy (§2). In both panels the orange and light-blue regions have a $1''$ and $2.5''$ radius, respectively, and mark the location of the BNS merger and its host galaxy.

object remnant of a BNS merger a few years after its birth.

1. Abbott, B. P. *et al.* Multi-messenger Observations of a Binary Neutron Star Merger. *Astrophys. J. Lett.* **848**, L12 (2017). 1710.05833.

2. Margutti, R. & Chornock, R. First Multimessenger Observations of a Neutron Star Merger. *arXiv e-prints* arXiv:2012.04810 (2020). 2012.04810.

3. Hajela, A. *et al.* Two Years of Nonthermal Emission from the Binary Neutron Star Merger GW170817: Rapid Fading of the Jet Afterglow and First Constraints on the Kilonova Fastest Ejecta. *Astrophys. J. Lett.* **886**, L17 (2019). 1909.06393.

4. Ryan, G., van Eerten, H., Piro, L. & Troja, E. Gamma-Ray Burst Afterglows in the Multimessenger Era: Numerical Models and Closure Relations. *Astrophys. J.* **896**, 166 (2020). 1909.11691.

5. Troja, E. *et al.* A thousand days after the merger: Continued X-ray emission from GW170817. *Mon. Not. R. Astron. Soc.* **498**, 5643–5651 (2020). 2006.01150.

6. Wang, H. & Giannios, D. Multimessenger Parameter Estimation of GW170817: From Jet Structure to the Hubble Constant. *Astrophys. J.* **908**, 200 (2021). 2009.04427.

7. Nakar, E. & Piran, T. Detectable radio flares following gravitational waves from mergers of binary neutron stars. *Nature* **478**, 82–84 (2011). 1102.1020.

8. Abbott, B. P. *et al.* GW170817: Observation of Gravitational Waves from a Binary Neutron Star Inspiral. *Phys. Rev. Lett.* **119**, 161101 (2017). 1710.05832.

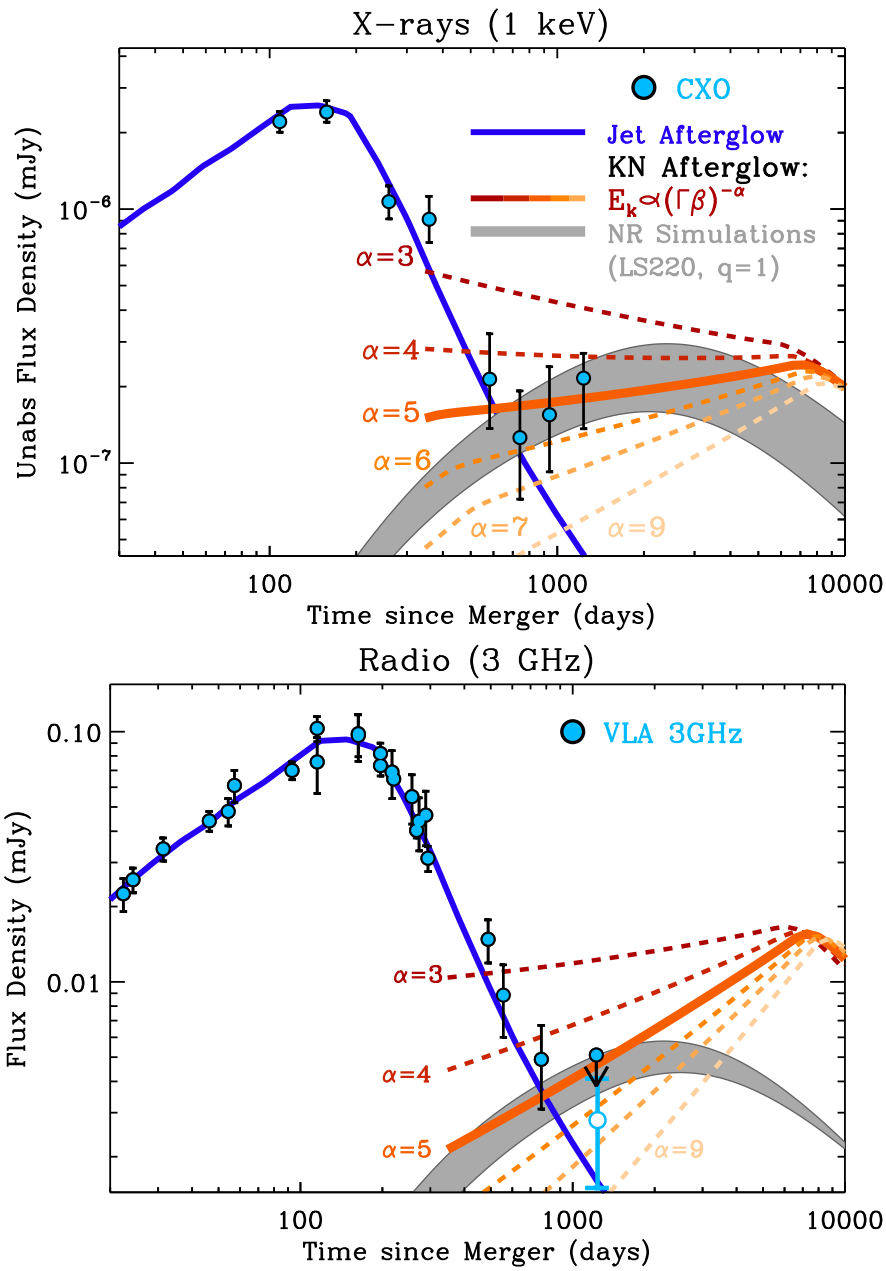

Figure 2 | X-ray and radio light-curves of GW170817 X-ray (*upper panel*) and radio (3 GHz, *lower panel*) evolution of the emission from GW170817 as detected by the *CXO* and the VLA (light-blue circles). Open circle: peak pixel flux value within one synthesized beam at the location of GW170817 from Balasubramanian et al.[26] At $\delta t > 900$ days the X-ray emission shows an excess compared to the off-axis jet afterglow model (solid blue line, §4 and §6) that indicates the emergence of a new emission component. Red-to-orange dashed lines: synchrotron radiation from the kilonova afterglow calculated using semi-analytical models[32] where we parametrized the kilonova kinetic energy distribution as $E_{\rm k} \propto (\Gamma\beta)^{-\alpha}$ for $\beta \geq 0.35$ and we used a total kilonova kinetic energy of 10^{51} erg. These models require $p < 2.15$ to avoid violating our radio upper limit. Here we use $p = 2.05$ and we emphasize with a solid thick line the $\alpha = 5$ model. Other kilonova afterglow parameters assumed: $\epsilon_B = 0.001$, $\epsilon_e = 0.1$, $n = 0.001\,{\rm cm}^{-3}$. Grey shaded area: synchrotron emission calculated from kilonova kinetic ejecta profiles derived from ab-initio numerical relativity simulations using a neutron-star mass-ratio $q = 1$ and the LS220 equation of state (§7). These simulations emphasize the contribution from the merger's dynamical ejecta. The shaded area corresponds to values $p_{KN} = 2.05 - 2.15$, $n = 6 \times 10^{-3}\,{\rm cm}^{-3}$, $\epsilon_e = 0.1$ and $\epsilon_B = 0.01$.

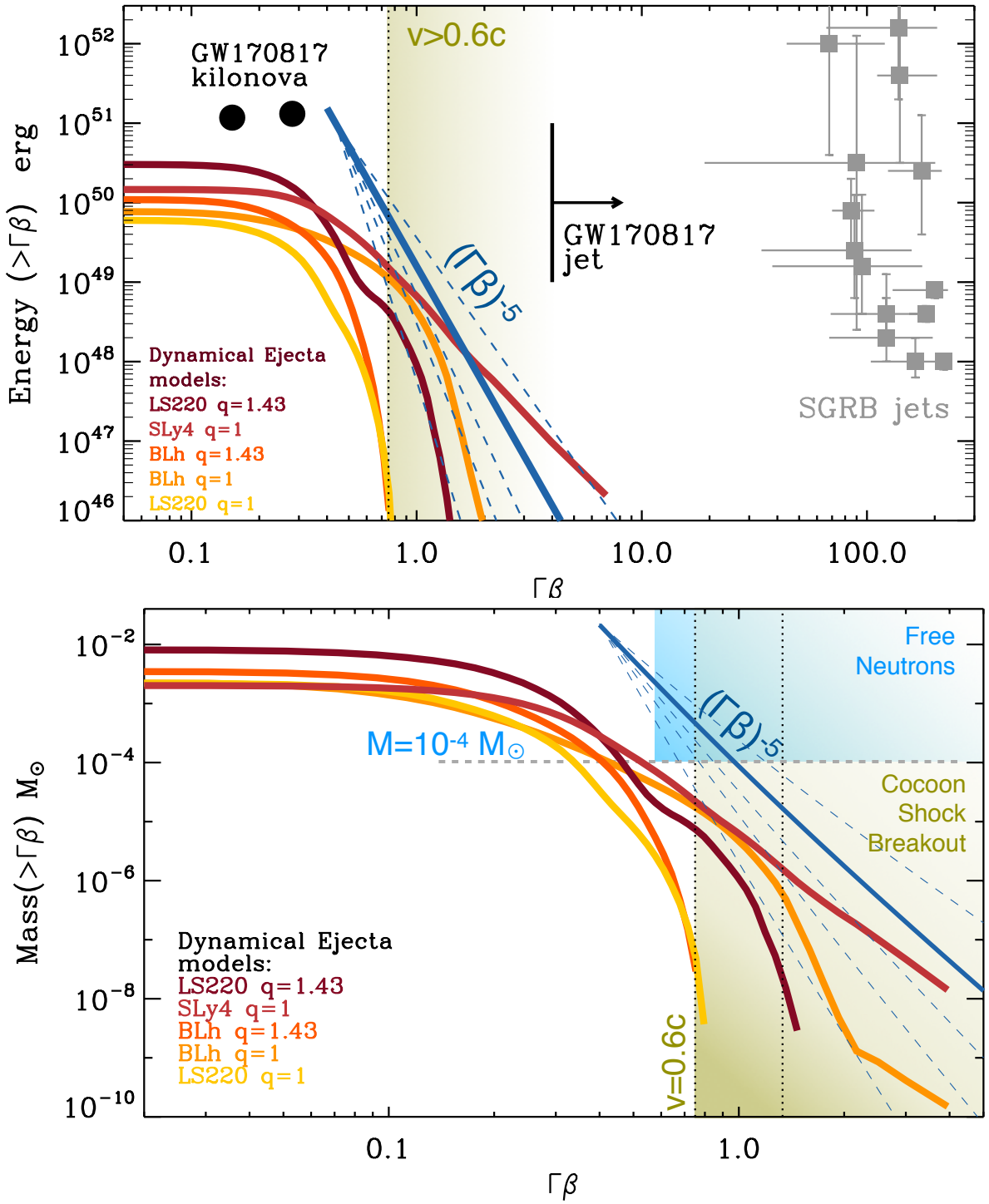

Figure 3 | **Kilonova kinetic energy and mass profiles** *Upper Panel:* Colored lines: kinetic energy profile of the fastest kilonova ejecta as a function of specific momentum $\Gamma\beta$. Dark-red to orange shade: dynamical ejecta profiles as inferred from ab-initio numerical-relativity simulations described in §7 for different EoS and NS mass ratios q. Blue lines: $E_{\rm KN}(>\Gamma\beta) \propto (\Gamma\beta)^{-\alpha}$ analytical profiles that include the contributions from all types of kilonova ejecta for $\alpha = 4, 5, 6, 7, 9$. Black filled circles: kinetic energy inferred from the modeling of the UV/optical/NIR kilonova emission.[11] Grey squares: SGRB jets.[55] *Lower Panel:* kilonova ejecta profiles in the mass phase-space. Colored area: region of the parameter space consistent with a cocoon shock breakout origin of GRB 170817A.[43]

9. Cantiello, M. *et al.* A Precise Distance to the Host Galaxy of the Binary Neutron Star Merger GW170817 Using Surface Brightness Fluctuations. *Astrophys. J. Lett.* **854**, L31 (2018). 1801.06080.

10. Metzger, B. D. Kilonovae. *Living Reviews in Relativity* **20**, 3 (2017). 1610.09381

11. Villar, V. *et al.* The combined ultraviolet, optical, and near-infrared light curves of the kilonova associated with the binary neutron star merger gw170817: Unified data set, analytic models, and physical implications. *Astrophys. J. Lett.* **851**, L21 (2017). 1710.11576

12. Cowperthwaite, P. S. *et al.* The Electromagnetic Counterpart of the Binary Neutron Star Merger LIGO/Virgo GW170817. II. UV, Optical, and Near-infrared Light Curves and Comparison to Kilonova Models. *Astrophys. J.* **848**, L17 (2017). 1710.05840

13. Drout, M. R. *et al.* Light curves of the neutron star merger GW170817/SSS17a: Implications for r-process nucleosynthesis. *Science* **358**, 1570–1574 (2017). 1710.05443.

14. Kilpatrick, C. D. *et al.* Electromagnetic evidence that SSS17a is the result of a binary neutron star merger. *Science* **358**, 1583–1587 (2017). 1710.05434.

15. Arcavi, I. The First Hours of the GW170817 Kilonova and the Importance of Early Optical and Ultraviolet Observations for Constraining Emission Models. *Astrophys. J. Lett.* **855**, L23 (2018). 1802.02164.

16. Waxman, E., Ofek, E. O., Kushnir, D. & Gal-Yam, A. Constraints on the ejecta of the GW170817 neutron star merger from its electromagnetic emission. *Mon. Not. R. Astron. Soc.* **481**, 3423–3441 (2018). 1711.09638.

17. Bulla, M. *et al.* The origin of polarization in kilonovae and the case of the gravitational-wave counterpart AT 2017gfo. *Nature Astronomy* **3**, 99–106 (2019). 1809.04078.

18. Nicholl, M. *et al.* Tight multi-messenger constraints on the neutron star equation of state from GW170817 and a forward model for kilonova light curve synthesis. *arXiv e-prints* arXiv:2102.02229 (2021). 2102.02229.

19. Mooley, K. P. *et al.* Superluminal motion of a relativistic jet in the neutron-star merger GW170817. *Nature* **561**, 355–359 (2018). 1806.09693.

20. Ghirlanda, G. *et al.* Compact radio emission indicates a structured jet was produced by a binary neutron star merger. *Science* **363**, 968–971 (2019). 1808.00469.

21. Hotokezaka, K. *et al.* A Hubble constant measurement from superluminal motion of the jet in GW170817. *Nature Astronomy* **3**, 940–944 (2019). 1806.10596.

22. Fong, W. *et al.* The Optical Afterglow of GW170817: An Off-axis Structured Jet and Deep Constraints on a Globular Cluster Origin. *Astrophys. J. Lett.* **883**, L1 (2019). 1908.08046.

23. Sari, R., Piran, T. & Halpern, J. P. Jets in Gamma-Ray Bursts. *Astrophys. J. Lett.* **519**, L17–L20 (1999). astro-ph/9903339.

24. Wu, Y. & MacFadyen, A. Constraining the Outflow Structure of the Binary Neutron Star Merger Event GW170817/GRB170817A with a Markov Chain Monte Carlo Analysis. *Astrophys. J.* **869**, 55 (2018). 1809.06843.

25. Duffell, P. C. & MacFadyen, A. I. A "Boosted Fireball" Model for Structured Relativistic Jets. *Astrophys. J. Lett.* **776**, L9 (2013). 1308.1731.

26. Balasubramanian, A. *et al.* Continued radio observations of GW170817 3.5 years post-merger. *arXiv e-prints* arXiv:2103.04821 (2021). 2103.04821.

27. Frail, D. A., Waxman, E. & Kulkarni, S. R. A 450 Day Light Curve of the Radio Afterglow of GRB 970508: Fireball Calorimetry. *Astrophys. J.* **537**, 191–204 (2000). astro-ph/9910319.

28. Piran, T. The physics of gamma-ray bursts. *Rev. Mod. Phys.* **76**, 1143–1210 (2004). astro-ph/0405503.

29. Sironi, L. & Giannios, D. A Late-time Flattening of Light Curves in Gamma-Ray Burst Afterglows. *Astrophys. J.* **778**, 107 (2013). 1307.3250.

30. Granot, J., Gill, R., Guetta, D. & De Colle, F. Off-axis emission of short GRB jets from double neutron star mergers and GRB 170817A. *Mon. Not. R. Astron. Soc.* **481**, 1597–1608 (2018). 1710.06421.

31. Nakar, E. The electromagnetic counterparts of compact binary mergers. *Phys. Rep.* **886**, 1–84 (2020). 1912.05659.

32. Kathirgamaraju, A., Tchekhovskoy, A., Giannios, D. & Barniol Duran, R. EM counterparts of structured jets from 3D GRMHD simulations. *Mon. Not. R. Astron. Soc.* **484**, L98–L103 (2019). 1809.05099.

33. Bell, A. R. The acceleration of cosmic rays in shock fronts - I. *Mon. Not. R. Astron. Soc.* **182**, 147–156 (1978).

34. Blandford, R. D. & Ostriker, J. P. Particle acceleration by astrophysical shocks. *Astrophys. J. Lett.* **221**, L29–L32 (1978).

35. Blandford, R. & Eichler, D. Particle acceleration at astrophysical shocks: A theory of cosmic ray origin. *Phys. Rep.* **154**, 1–75 (1987).

36. Radice, D. & Rezzolla, L. THC: a new high-order finite-difference high-resolution shock-capturing code for special-relativistic hydrodynamics. *Astron. & Astrophys.* **547**, A26 (2012). 1206.6502.

37. Radice, D., Rezzolla, L. & Galeazzi, F. Beyond second-order convergence in simulations of binary neutron stars in full general relativity. *Mon. Not. R. Astron. Soc.* **437**, L46–L50 (2014). 1306.6052.

38. Radice, D., Rezzolla, L. & Galeazzi, F. High-order fully general-relativistic hydrodynamics: new approaches and tests. *Class. & Quant. Grav.* **31**, 075012 (2014). 1312.5004.

39. Goldstein, A. *et al.* An Ordinary Short Gamma-Ray Burst with Extraordinary Implications: Fermi-GBM Detection of GRB 170817A. *Astrophys. J. Lett.* **848**, L14 (2017). 1710.05446.

40. Savchenko, V. *et al.* INTEGRAL Detection of the First Prompt Gamma-Ray Signal Coincident with the Gravitational-wave Event GW170817. *Astrophys. J. Lett.* **848**, L15 (2017). 1710.05449.

41. Metzger, B. D., Bauswein, A., Goriely, S. & Kasen, D. Neutron-powered precursors of kilonovae. *Mon. Not. R. Astron. Soc.* **446**, 1115–1120 (2015). 1409.0544.

42. Bromberg, O., Tchekhovskoy, A., Gottlieb, O., Nakar, E. & Piran, T. The γ-rays that accompanied GW170817 and the observational signature of a magnetic jet breaking out of NS merger ejecta. *Mon. Not. R. Astron. Soc.* **475**, 2971–2977 (2018). 1710.05897.

43. Gottlieb, O., Nakar, E., Piran, T. & Hotokezaka, K. A cocoon shock breakout as the origin of the γ-ray emission in GW170817. *Mon. Not. R. Astron. Soc.* **479**, 588–600 (2018). 1710.05896.

44. Granot, J., Guetta, D. & Gill, R. Lessons from the Short GRB 170817A: The First Gravitational-wave Detection of a Binary Neutron Star Merger. *Astrophys. J. Lett.* **850**, L24 (2017). 1710.06407.

45. Margalit, B. & Metzger, B. D. Constraining the Maximum Mass of Neutron Stars from Multi-messenger Observations of GW170817. *Astrophys. J. Lett.* **850**, L19 (2017). 1710.05938.

46. Shibata, M. *et al.* Modeling GW170817 based on numerical relativity and its implications. *Phys. Rev. D* **96**, 123012 (2017). 1710.07579.

47. Metzger, B. D., Thompson, T. A. & Quataert, E. A Magnetar Origin for the Kilonova Ejecta in GW170817. *Astrophys. J.* **856**, 101 (2018). 1801.04286.

48. Rezzolla, L., Most, E. R. & Weih, L. R. Using Gravitational-wave Observations and Quasi-universal Relations to Constrain the Maximum Mass of Neutron Stars. *Astrophys. J. Lett.* **852**, L25 (2018). 1711.00314.

49. Gill, R., Nathanail, A. & Rezzolla, L. When Did the Remnant of GW170817 Collapse to a Black Hole? *Astrophys. J.* **876**, 139 (2019). 1901.04138.

50. Ciolfi, R. Collimated outflows from long-lived binary neutron star merger remnants. *Mon. Not. R. Astron. Soc.* **495**, L66–L70 (2020). 2001.10241.

51. Murguia-Berthier, A. *et al.* The Fate of the Merger Remnant in GW170817 and Its Imprint on the Jet Structure. *Astrophys. J.* **908**, 152 (2021). 2007.12245.

52. Fender, R. P., Belloni, T. M. & Gallo, E. Towards a unified model for black hole X-ray binary jets. *Mon. Not. R. Astron. Soc.* **355**, 1105–1118 (2004). astro-ph/0409360.

53. Gladstone, J. C., Roberts, T. P. & Done, C. The ultraluminous state. *Mon. Not. R. Astron. Soc.* **397**, 1836–1851 (2009). 0905.4076.

54. Körding, E., Colbert, E. & Falcke, H. A radio monitoring survey of ultra-luminous X-ray sources. *Astron. & Astrophys.* **436**, 427–436 (2005). astro-ph/0502265.

55. Wu, Y. & MacFadyen, A. GW170817 Afterglow Reveals that Short Gamma-Ray Bursts are Neutron Star Mergers. *Astrophys. J. Lett.* **880**, L23 (2019). 1905.02665.

Correspondence Correspondence and requests for materials should be addressed to A.H. (email: ahajela@u.northwestern.edu).

Acknowledgements A. Hajela is partially supported by a Future Investigators in NASA Earth and Space Science and Technology (FINESST) award # 80NSSC19K1422. This research was supported in part by the National Science Foundation under Grant No. AST-1909796 and AST-1944985, by NASA through Chandra Award Number G09-20058A and through Space Telescope Science Institute program #15606. K. D. Alexander is supported by NASA through NASA Hubble Fellowship grant #HST-HF2-51403.001-A awarded by the Space Telescope Science Institute, which is operated by the Association of Universities for Research in

Astronomy, Inc., for NASA, under contract NAS5-26555. B. D. Metzger is supported by NSF grant AST-2002577 and NASA grants 80NSSC20K0909, NNX17AK43G. A. Kathirgamaraju acknowledges support from the Gordon and Betty Moore Foundation through Grant GBMF5076. D. Radice acknowledges support from the U.S. Department of Energy, Office of Science, Division of Nuclear Physics under Award Number(s) DE-SC0021177 and from the National Science Foundation under Grant No. PHY-2011725. S. Bernuzzi acknowledges support by the EU H2020 under ERC Starting Grant, no. BinGraSp-714626. L. Sironi acknowledges support from the Sloan Fellowship, the Cottrell Scholars Award, NASA 80NSSC18K1104 and NSF PHY-1903412. I. Heywood acknowledges support from the UK Science and Technology Facilities Council [ST/N000919/1] and the South African Radio Astronomy Observatory which is a facility of the National Research Foundation (NRF), an agency of the Department of Science and Innovation. B. Margalit is supported by NASA through NASA Hubble Fellowship grant No. HST-HF2-51412.001-A awarded by the Space Telescope Science Institute, which is operated by the Association of Universities for Research in Astronomy, Inc., for NASA under contract NAS5-26555. R. Barniol Duran acknowledges support from National Science Foundation (NSF) under grant 1816694. V. A. Villar is supported by the Simons Foundation through a Simons Junior Fellowship (#718240). M. Nicholl is supported by a Royal Astronomical Society Research Fellowship and by the European Research Council (ERC) under the European Union's Horizon 2020 research and innovation programme (grant agreement No. 948381). The Berger Time Domain group at Harvard is supported in part by NSF and NASA grants, as well as by the NSF under Cooperative Agreement PHY-2019786 (The NSFAI Institute for Artificial Intelligence and Fundamental Interactions http://iaifi.org/).

The scientific results reported in this article are based to a significant degree on observations made by the *Chandra* X-ray Observatory, and the data obtained from the Chandra Data Archive. Partial support for this work was provided by the National Aeronautics and Space Administration through Chandra Award Number GO1-22075X issued by the Chandra X-ray Center, which is operated by the Smithsonian Astrophysical Observatory for and on behalf of the National Aeronautics Space Administration under contract NAS8-03060. The National Radio Astronomy Observatory is a facility of the National Science Foundation operated under cooperative agreement by Associated Universities, Inc. The MeerKAT telescope is operated by the South African Radio Astronomy Observatory, which is a facility of the National Research Foundation, an agency of the Department of Science and Innovation.

Competing Interests The authors declare that they have no competing financial interests.

Methods

1 *Chandra X-ray Observatory* (*CXO*) Observations

We present new *CXO* observations of the X-ray emission from GW170817 acquired at $\delta t = 1209$ – 1258 days since merger and a complete and homogeneous analysis of the entire *CXO* data set. Results from *CXO* observations of the jet afterglow of GW170817 in the time range $\delta t = 2.33$ – 939.31 days have already been published in the literature.[3,5,56–67] With respect to previous data reductions: (1) when possible, we do not assume a spectral model for the X-ray count-to-flux calibration, which allows us to test for spectral evolution; (2) we align all the X-ray images to a common astrometric solution, significantly improving on the *CXO* relative astrometry; (3) for each observation we extract a spectrum and we perform a flux calibration that utilizes the complete information on the instrumental response at the time of the observation (as opposed to using averaged instrumental responses); (4) we jointly fit spectra from observations acquired close in time (i.e. around the same "epoch") as opposed to merging the files into an average spectrum; (5) we implement an accurate point-spread function (PSF) correction; (6) we calculate the model parameter uncertainties (including the unabsorbed fluxes) with MCMC simulations that self-consistently account for the low-count statistics and the deviation from Gaussian statistics.

Observations at $\sim$ 3.4 years post-merger We observed GW170817 with the *CXO* from December 09, 2020 at 00:05:21 UT through December 13, 2020 at 14:02:43 UT, and further between January 18, 2021 at 09:43:15 UT and January 27, 2021 at 08:49:13 UT, spanning $\delta t \sim 1209$ – 1258 days after the merger. The observation was taken in seven distinct exposures (Obs ID

22677, 24887, 24888, 24889, 23870, 24923, and 24924; PI Margutti; programs #21510449 and #22510329, publicly available on the *CXO* archive) for a total exposure time of ~ 189.1 ks.

Data Analysis We reprocessed the *CXO* data using the `repro` task within `CIAO` (v4.13.0[68]) with standard ACIS data filtering and using the latest calibration database (`CALDB, v4.9.4`). We used `wcs_match` and `wcs_update` to realign all the IDs to a common astrometric solution using as a reference the list of X-ray point-source positions generated with `wavdetect` run on our longest exposure observation (Obs ID 20860). In ID 20860 the X-ray emission from GW170817 is detected with high significance at sky coordinates RA=$13^h09^m48^s.061 \pm 0.049^s$ and dec=-23°:22′:52.88″ $\pm$ 0.034″ (J2000). After having realigned the images, for each ID we extracted source count-rates and spectra using a 1″ region centered at the coordinates above. Extended Data Table 1 lists the inferred 0.5 – 8 keV net count-rates and the associated targeted-detection significance. For source detection, we employed a 1″ source region and we filtered in the energy range 0.5 – 8 keV to minimize the background contribution. For reference, a 1″ region contains $\gtrsim 90\%$ of the PSF at 1 keV.

For the observations at $\delta t \sim 939$ days, an X-ray source is clearly detected at the location of GW170817 with a statistical significance of $\sim 5.4\,\sigma$ (Gaussian equivalent), corresponding to a net count-rate of $(7.53 \pm 2.93)\times10^{-5}$ cts s^{-1} (0.5 – 8 keV). For the four observations acquired at $\delta t \sim 1205$ – 1214 days, we find that the observed net count-rate is $(1.13 \pm 0.36)\times10^{-4}$ cts s^{-1} ($\sim 6.3\,\sigma$ detection significance), whereas for the remaining observations acquired between $\delta t \sim 1250$ – 1258 days, the observed net count-rate is $(4.31 \pm 2.28)\times10^{-5}$ cts s^{-1} and an X-ray source is detected at a significance level of $\sim 3.4\,\sigma$. Being temporally close, we combined the latter

two sets of observations spanning 1205 – 1258 days and we infer a net count-rate of $(7.68 \pm 2.12) \times 10^{-5}\,\mathrm{cts\,s^{-1}}$, where an X-ray source is detected with a $\sim 7.2\,\sigma$ statistical significance.

For each re-aligned Obs ID we extracted a spectrum using a $1''$ circular source region centered at the location of the X-ray counterpart of GW170817 indicated above and a source-free background region of $22''$. We used `specextract`, setting the `refcoord` parameter to the center of the source region to ensure an accurate PSF correction to the inferred fluxes. We note that removing this explicit `refcoord` parameter setting leads to an overestimate of the PSF correction by an average factor of $\approx 1.2 - 1.5$ for a source region of $1''$. This procedure furthermore ensures that the appropriate instrumental ARF (Auxiliary Response File) and RMF (Redistribution Matrix File) response files are generated for each Obs ID. We fitted the data with an absorbed power-law spectral model (`tbabs*ztbabs*cflux(pow)` within *Xspec*, v12.9.1p). We adopted a Galactic neutral hydrogen column density[69] in the direction of GW170817 of $\mathrm{NH_{gal}} = 7.84 \times 10^{20}\,\mathrm{cm^{-2}}$. Consistent with results from previous analysis,[3,56,58,59,67] we did not find evidence for intrinsic absorption and we thus assumed $\mathrm{NH_{int}} = 0\,\mathrm{cm^{-2}}$ in the following analysis. For $\delta t < 750$ days, we jointly fitted the observations acquired around the same epoch since merger leaving the spectral photon index, Γ, and the unabsorbed 0.3 – 10 keV flux as free parameters. We fitted the data in the 0.3 – 10 keV energy range. We note that filtering the data in the 0.5 – 8 keV energy range before fitting does not lead to significantly different inferences. We used the Cash statistics and we employed a chain of 10^5 MCMC simulations to estimate the parameter uncertainties to account for the deviation from Gaussian statistics in the regime of low counts. The results from our X-ray spectral modeling are reported in Extended Data Table 1. We find no evidence for X-ray spectral

evolution of the source at $\delta t < 745$ days. From a joint spectral fit of all *CXO* observations at $\delta t < 745$ days with the same Γ we infer a best-fitting $\Gamma = 1.603^{+0.102}_{-0.076}$, consistent with our previous analysis of these observations,[3] which used a previous CALDB v4.8.3 and a $1.5''$ source region.

We now consider the *CXO* observations acquired at $\delta t > 745$ days. These *CXO* observations were acquired in two epochs at $\delta t \sim 939$ and $\delta t \sim 1234$ days since merger. The low-count statistics of 6 and 12 photons, respectively, available for model fitting after *Xspec* filtering in the 0.3 – 10 keV energy range leads to poorly constrained spectral photon indexes $\Gamma = 1.16^{+1.38}_{-1.39}$ and $\Gamma = 1.92^{+2.53}_{-0.65}$. We thus proceeded by freezing the spectral photon index to $\Gamma = 1.603$ (i.e. the best-fit value inferred from the joint fit of all the *CXO* data collected at $\delta t < 745$ days) for the purpose of count-to-flux calibration. The inferred unabsorbed 0.3 – 10 keV flux is $F_{\rm x} = 1.81^{+0.79}_{-0.94} \times 10^{-15}\,{\rm erg\,cm^{-2}\,s^{-1}}$ at $\delta t \sim 939$ days, and $F_{\rm x} = 2.47^{+0.62}_{-0.91} \times 10^{-15}\,{\rm erg\,cm^{-2}\,s^{-1}}$ at $\delta t \sim 1234$ days, corresponding to luminosities of $L_{\rm x} \approx (3-5) \sim 10^{38}\,{\rm erg\,s^{-1}}$ (Extended Data Table 1).

We end by addressing the possibility of X-ray spectral evolution at $\delta t > 745$ days. We assessed the statistical evidence for X-ray spectral evolution in two ways. First, from a joint spectral modeling of all *CXO* data acquired at $\delta t > 745$ days with a power-law spectrum, we infer $\Gamma = 1.54^{+0.83}_{-0.75}$. Compared to $\Gamma = 1.603^{+0.102}_{-0.076}$ of the earlier X-ray data reported above, we find that there is no evidence for statistically significant X-ray spectral evolution from this analysis. Second, we generated 10^6 synthetic spectra of $N = 12$ photons (as observed at $\delta t \sim 1234$ days in the 0.3 – 10 keV energy range after *Xspec* filtering) by randomly sampling the probability density distribution associated with an incoming $\Gamma = 1.6$ spectrum with $NH_{\rm gal} = 0.0784 \times 10^{22}\,{\rm cm^{-2}}$ convolved with the *CXO* instrumental response. We applied the non-parametric distribution-free Epps–Singleton

two-sample test to each sample and the parent distribution and we found that $\sim 52\%$ of the synthetic samples have a p-value at least as extreme as the one associated with the observed photon distribution, leading to no statistical evidence of a departure of the detected photon distribution at $\delta t > 745$ days from earlier X-ray data. We conclude that there is no statistically significant evidence for the evolution of the X-ray spectrum at $\delta t > 745$ days.

Finally, we compare the results from our X-ray analysis with previous results that appeared in the literature, and specifically with the analyses by Troja et al. 2020[5] (for $\delta t \sim 582$ – 945 days) and Makhathini et al. 2020[67] (for $\delta t \sim 9$ – 745 days). The analysis by Makhathini et al. 2020 cannot be used to test for X-ray spectral evolution of the source because the final count-to-flux calibration is performed by assuming a spectral photon index. We find that the central values of the X-ray fluxes reported by Makhathini et al. 2020 using a $1''$ source region are systematically larger than our fluxes (by a factor of up to 30%). Discrepancy remains even after adopting the same $\Gamma = 1.57$ for the count-to-flux calibration. We are able to reproduce the Makhathini et al., X-ray fluxes by removing the `refcoord` parameter setting from `specextract`, which leads to artificially inflated PSF corrections of $\approx$ 20–50%, as previously noted. Our X-ray fluxes in the time range $\delta t \sim 582$ – 945 days are consistent with those reported by Troja et al. 2020 within 1-σ uncertainties. We found that we could reproduce the Troja et al. 2020 fluxes by using the online Portable Interactive Multi-Mission Simulator (PIMMS) for the count-rate to flux calibration. In contrast, our spectral analysis and count-to-flux calibration is based on ARFs and RMFs generated from each individual Obs ID to best account for the instrumental response at the time and in the

conditions of the observation, as opposed to the proposal planning tool PIMMS.*

2 VLA Observations

We initiated late-time S and Ku-band Karl G. Jansky Very Large Array (VLA) observations of GW170817 as part of our joint Chandra-VLA proposals #21510449 and #22510329 (PI Margutti). GW170817 was observed for a total of 10.21 hours on source at S-band spread between three observations occurring on 15th December 2020 ($\delta t = 1216.08$), 27th December 2020 ($\delta t = 1228.02$) and 2nd February 2021 ($\delta t = 1264.95$). All three observations were conducted while the VLA was in A-configuration and at a central frequency of $3\,\mathrm{GHz}$ using a $2\,\mathrm{GHz}$ bandwidth.

Additionally, we conducted a single observation at Ku-band on 10th February 2021 (δt=1272.88) for a total of 2.74 hours on source. The observation was conducted with the VLA in A-configuration and at a central frequency of $15\,\mathrm{GHz}$ using a $6\,\mathrm{GHz}$ bandwidth.

These data are publicly available on the VLA archive under project IDs SL0449 and SM0329. Details of each observation are given in Extended Data Table 2.

Data Analysis and Imaging Each individual observation was independently calibrated using the VLA calibration pipeline version 2020.1.0.36 as part of CASA version[70] 6.1.2.7, with 3C286 used as the flux density and bandpass calibrator and J1258-2219 used to calibrate the time-varying complex gains. We then manually inspected and validated the output and re-ran the pipeline after flagging additional radio frequency interference (RFI). Additional RFI flagging was performed on

*https://cxc.harvard.edu/ciao/why/pimms.html

the results of the second pipeline run. In order to achieve maximum sensitivity we combined the three epochs of S-band data into a single measurement set using the CASA task CONCAT. We imaged the concatenated data using `wsclean`,[71,72] creating a 16384×16384 pixel image with a single pixel corresponding to $0.08''$. The synthesised beam is $1.19'' \times 0.66''$ with a position angle of -5.57 degrees. In order to account for spectral variation introduced for sources far from the phase center (we are imaging well beyond the half power point of the primary beam) we fit a third order polynomial (`fit-spectral-pol 4`) over eight output channels (`channels-out 64`). No time or frequency averaging was performed when imaging in order to avoid bandwidth or temporal smearing of sources far from the phase center ensuring the best possible deconvolution. We performed one round of phase-only self-calibration using a sky-model produced from our phase reference calibrated data.

We do not detect any significant emission at the position of GW170817. The root-mean-square (RMS) noise at the edge of the image in a region free of sources is $\sim 1.2\,\mu$Jy while in a circular region with 25 pixel radius centered on the position of GW170817 we measure an RMS noise of $\sim 1.7\,\mu$Jy.

The single Ku-band epoch was calibrated using the VLA calibration pipeline version 2020.1.0.36 as part of CASA version 6.1.2.7 and validated by NRAO as part of the Science Read Data Products project. We imaged the calibrated measure set using the CASA task `tclean` with a user defined mask. We created a 2048×2048 pixel image with a cell size of $0.02''$. We do not detect any significant emission at the location of GW170817 and measure an RMS noise of $1.7\,\mu$Jy in a 30×30 pixel region centred on the position of GW170817.

3 MeerKAT Observations

We conducted a single observation of the field of GW170817 with the MeerKAT radio interferometer on the 3rd January 2021 as part of a DDT request (DDT-20201218-JB-01). These data are available publicly on the SARAO archive. Data were recorded for a total of 7.56 hours (resulting in 7.24 hours on source) with an $8\,\mathrm{s}$ dump time at the UHF band between $544\,\mathrm{MHz}$ and $1088\,\mathrm{MHz}$ with a central frequency of $816\,\mathrm{MHz}$ using 4096 frequency channels. Details of the observation are given in Extended Data Table 2.

Data Analysis and Imaging Data reduction was performed using OXKAT, a suite of semi-automated containerised scripts to reduce MeerKAT UHF and L-band data.[73] First, phase reference calibration (1GC) is carried out using CASA, with flagging performed with Tricolour (a variant of the SARAO Science Data Processing flagging software). B0407−65 was observed to calibrate the flux and bandpass of the instrument and 3C283 was used to calibrate the time variable complex gains. Second, we used WSCLEAN to image the field and the resulting sky model was used to perform phase and delay self-calibration (2GC) using CUBICAL[74]. Images created throughout this process are 10240 by 10240 pixels with a robust weighting of −0.5 and pixel size of 1.7 arcseconds. The phase calibrator, 3C283, is a bright off-axis source when observing GW170817 with MeerKAT at the UHF band and leaves strong imaging artefacts after 2GC calibration. Strong sources away from the phase center of an interferometer have their apparent spectral shape modified by the time and frequency dependent primary beam, and for sufficiently wide field of view one set of gain solutions (direction-dependent) is not appropriate to properly calibrate the data. These issues result in a corrupted point spread function that will not vanish under deconvolution. The

primary beam can be corrected for either by providing a model of the primary beam for the array, or by using higher order polynomials when fitting the spectral variation when cleaning (OXKAT employs the latter). To correct for direction-dependent gains across the wide MeerKAT field of view ($\sim 2\,\mathrm{deg}^2$ at UHF) we 'peel' the source 3C283, and performed faceted direction dependent self-calibration on the residual data. The peeling stage was performed using CUBICAL[74], and the facet based direction dependent calibration was carried out using KILLMS with DDFACET[75] used to image the corrected data. To enhance the resolution we image the final data-set with a Briggs robustness parameter -1.

The RMS noise at the edge of the image in a region free of sources is $8.5\,\mu\mathrm{Jy}$. Due to the extremely high source brightness sensitivity of MeerKAT the region around the phase center has a very high density of sources, making it difficult to estimate the phase center noise. We opt to fit the entire image for significant emission using PyBDSF[76] using a island and pixel threshold of three and five sigma, respectively, with adaptive RMS thresholding turned on. We identify extended (resolved) emission from the host galaxy of GW170817 (NGC 4993) and emission from a source. We identify no significant emission at the position of GW170817. Using a 40×40 pixel region centered on the position of GW170817 we measure an RMS noise of $\sim 13\,\mu\mathrm{Jy}$.

4 Evidence for an X-ray Excess of Emission

We first assessed the statistical evidence of an excess of X-ray emission with respect to the off-axis jet afterglow model by fitting the post-peak multi wavelength afterglow decay with the following model $F_\nu \propto \nu^{-\beta} t^{-\alpha}$. The X-ray to radio emission of GW170817 is powered by syn-

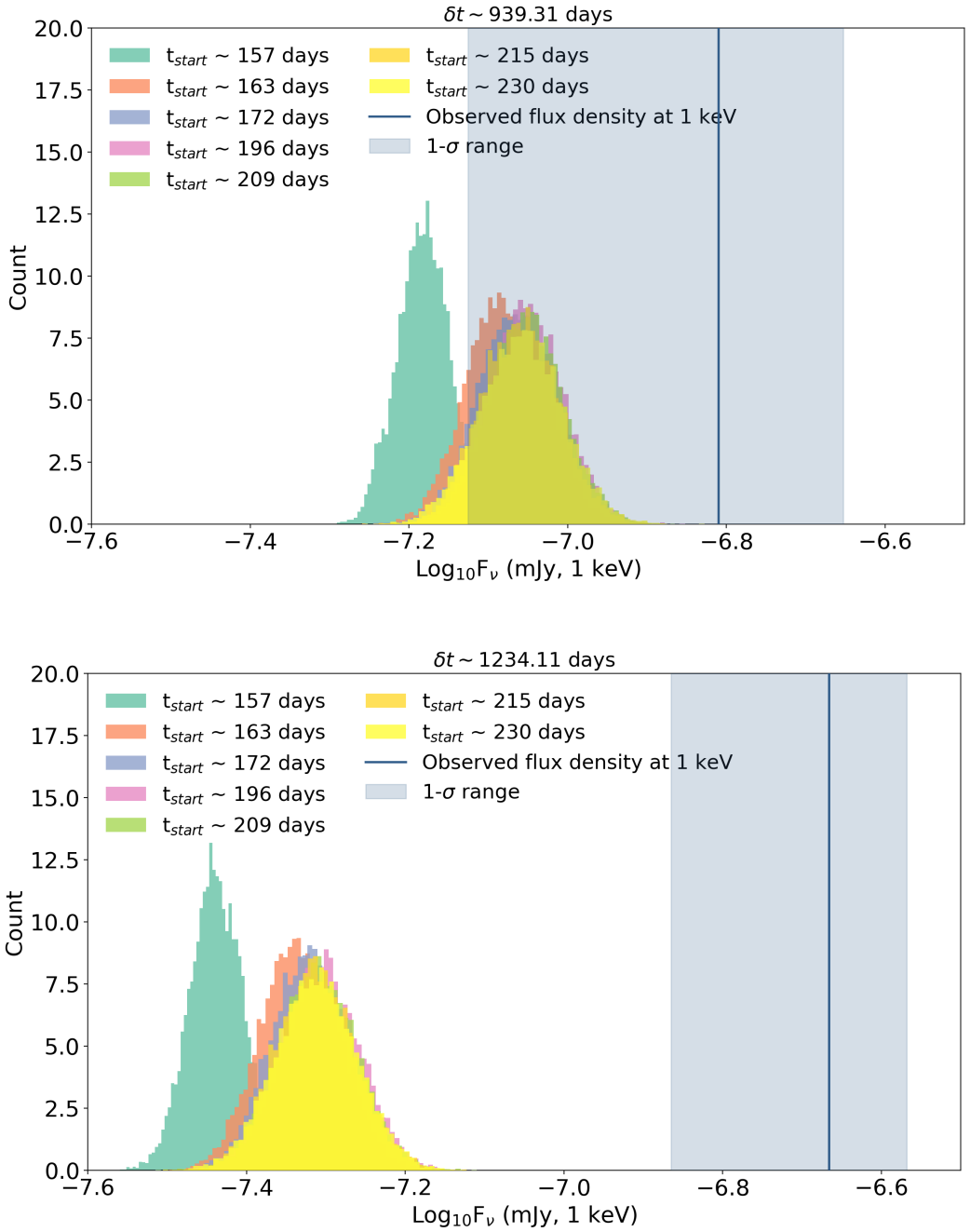

Extended Data Figure 1 | Universal post jet-break model flux distributions: *Top Panel:* Expected 1-keV flux density distributions at 939.31 days (histograms in color) derived from fitting the post-peak multi-wavelength afterglow of GW170817 in the post jet-break regime with $F_\nu \propto \nu^{-\beta} t^{-\alpha}$ (where $\beta = (p-1)/2$ and $\alpha = p$) in the time range $t_{\rm start} < \delta t < 900$ days for a variety of choices of $t_{\rm start}$. Vertical blue thick line and shaded area: observed X-ray flux density at this epoch and $\pm 1\,\sigma$ confidence range. *Bottom Panel:* Same as the top panel for 1234 days since merger.

chrotron radiation in the optically thin regime[22,59] for which $\beta = (p-1)/2$, where p is the power-law index of the relativistic electron distribution $dN_{\rm e}/d\gamma_{\rm e} \propto \gamma_{\rm e}^{-p}$ above some minimum Lorentz factor $\gamma_{\rm min}$. Standard closure relations[77] in the post jet break phase, which apply to the post-peak afterglow evolution, imply $\alpha = p$.[23] Our model is thus: $F_\nu \propto \nu^{-(p-1)/2} t^{-p}$ (we call it "universal post jet-break model"). The multi-wavelength jet afterglow of GW170817 peaked at $t_{\rm pk} \approx 160$ days.[58,78,79] We fitted the multi-wavelength post-peak jet afterglow evolution with the model above in the time range $t_{\rm start} < \delta t < 900$ days for several choices of start time $t_{\rm start} = 157, 163, 172, 196, 209, 215, 230$ days. We used VLA observations at 3 and 6 GHz compiled from references[3,19,58,59,78,80–82]; *Hubble Space Telescope* (HST) observations at optical wavelengths from reference[22]; and CXO observations at 1 keV from this work.

We employed MCMC sampling with a Python module, `emcee`[83]. For each choice of $t_{\rm start}$ we sampled 10^5 times the expected X-ray flux density distribution at 1 keV ($F_{1\,\rm keV}$) at the times of the last two *CXO* epochs at $t_1 = 939.31$ days and $t_2 = 1234.11$ days (Extended Data Table1, Extended Data Figure 1). For each sample we converted the predicted 1-keV flux densities ($F_{1\,\rm keV,1} \equiv F_{1\,\rm keV}(t_1)$ and $F_{1\,\rm keV,2} \equiv F_{1\,\rm keV}(t_2)$) into observed $0.5-8$ keV total (i.e. source plus background) counts in a $1''$ region (c_1 and c_2) using the respective exposure times, the count-to-flux conversion factors derived from *Xspec* and the observed background. We computed for each sample i the probabilities $P_{\rm i,1} \equiv Poisson(c \geq N_{\rm obs,1}|c_1)$ and $P_{\rm i,2} \equiv Poisson(c \geq N_{\rm obs,2}|c_2)$, which represent the probability of each sample to produce a number of X-ray photons larger or equal to those observed at t_1 and t_2 after *Xspec* filtering in the $0.5-8$ keV energy band ($N_{\rm obs,1} = 6$ and $N_{\rm obs,2} = 12$) as a result of a Poissonian fluctuation. For each model defined by the choice of t_{start}, the

total probability to lead to a deviation at least as prominent as the one observed at t_1 and t_2 is the re-normalized sum of the sample probabilities: $P_1 = \frac{1}{N_{\rm sample}} \sum_i P_{\rm i,1}$ and $P_2 = \frac{1}{N_{\rm sample}} \sum_i P_{\rm i,2}$. We find that the resulting P_1 and P_2 vary in the range $P_1 = 0.060$ – 0.139 and $P_2 = 2.61 \times 10^{-4}$ – 1.53×10^{-3} depending on the choice of $t_{\rm start}$. The observed X-rays at 1234 days thus correspond to a $3.2\,\sigma$ – $3.7\,\sigma$ (Gaussian equivalent) deviation from the off-axis jet model. The combined chance probability to obtain deviations from the off-axis jet model at least as prominent as those observed at 939.31 days and 1234.11 days is $P = 1.73 \times 10^{-5}$ – 2.50×10^{-4}. We conclude that the observed X-rays at $\delta t > 900$ days represent a $3.6\,\sigma$ – $4.3\,\sigma$ (Gaussian equivalent) deviation from the universal post jet-break model that best fits earlier observations across the electromagnetic spectrum.

We further performed a similar statistical study to test the excess of X-ray emission with respect to the off-axis structured jet light-curves modeled with `JetFit`.[24,25,84] `JetFit` fits the afterglow light curves for arbitrary viewing angles using a 'boosted-fireball' structured jet model to compute the jet dynamics as it spreads. It naturally accommodates a diverse range of outflows from mildly-relativistic quasi-spherical outflows to ultra-relativistic highly collimated jets. `JetFit` uses the python package `emcee` to explore the full parameter space formed by eight parameters: the explosion energy, E_0; the ambient density, n; the asymptotic Lorentz factor, η_0; the boost Lorentz factor, $\gamma_{\rm B}$; the spectral index of the electron distribution, p; the electron energy fraction, $\epsilon_{\rm e}$; the magnetic energy fraction, $\epsilon_{\rm B}$; and viewing angle $\theta_{\rm obs}$; and find the best-fitting values and their posterior distributions. Because the broadband SED of GW170817, from $\delta t \sim 2 - 745$ days, is best explained by a simple power-law, some of these parameters are highly degenerate and the problem is under-constrained. Hence, we fixed $\epsilon_{\rm e} = 0.1$, as predicted from the simulations of par-

ticle acceleration by relativistic shocks,[85] $n = 0.01\,\mathrm{cm}^{-3}$, the upper-limit on the ambient density inferred from the study of the host X-ray thermal emission,[3] and $\gamma_{\rm B} = [7, 10, 12]$. We selected these $\gamma_{\rm B}$ values based on the VLBI measurements of the angular displacement of the radio emission with time, which constrained the jet Lorentz factor $\Gamma \approx 4$ at the time of the afterglow peak[79] (or $\theta_{\rm obs} - \theta_{\rm j} \approx 1/\Gamma \approx 1/4$).[†] We use `JetFit` to fit the multi-wavelength afterglow light-curves at 3 GHz, 6 GHz, optical and at 1 keV frequencies acquired at $2 < \delta t < 900$ days. The jet opening angle $\theta_{\rm j}$ of GW170817 has been estimated to be of the order of a few degrees,[19,20] and we thus consider the $\gamma_{\rm B} = 12$ boosted fireball model as our fiducial case. The best-fitting light curves and the one- and two-dimensional projections of the posterior distribution of the free parameters for $\gamma_{\rm B} = 12$ are shown in Extended Data Figure 2.

We use the full posterior distribution of all the free parameters to compute the distribution of flux density at 1 keV at t_1 and t_2 for models with $\gamma_{\rm B} = [7, 10, 12]$. Similar to the above statistical analysis, we convert these flux densities to the total counts in the 0.5 – 8 keV energy range in a $1''$ region, calculate the probability of each sample, i, $P_{\rm i,j} = Poisson(c \geq N_{\rm obs,j}|c_{\rm j})$, where $\rm j \in 1, 2$ for the two epochs respectively, and finally compute the cumulative probabilities, $P_{\rm j}$, to lead to a deviation at least as prominent as the one observed at t_1 and t_2 (Extended Data Figure 3). For different values of γ_B, we find $P_{\rm j}$ in the range $P_1 = 0.07$ – 0.15 and $P_2 = 7.36 \times 10^{-4}$ – 2.82×10^{-3}, corresponding to a $2.9\,\sigma$ – $3.4\,\sigma$ (Gaussian equivalent) deviation of the observed X-rays at 1234 days from the light-curve modeled by the off-axis structured jet model. We further find the com-

[†] `JetFit` can reliably predict the afterglow from boosted fireballs with $\gamma_{\rm B} \leq 12$, which translates into $\theta_{\rm j} \approx 1/\gamma_{\rm B} \geq 4.8°$

bined chance probability of $P = 5.59 \times 10^{-5}$ – 4.69×10^{-4} to obtain deviations from the off-axis structured jet model at least as prominent as those observed at t_1 and t_2, corresponding to a $3.5\,\sigma$ – $4.0\,\sigma$ (Gaussian equivalent) deviation from the light-curve modeled by the off-axis structured jet model. Larger γ_B values imply a higher level of collimation of the jet, and hence a faster post-peak transition to the asymptotic power-law decay, which explains the highest significance of the excess associated to the $\gamma_B = 12$ model (Extended Data Figure 3). Since for GW170817 $\theta_j \leq 5^\circ$ and our most collimated model has $\gamma_B = 12$ (i.e. $\theta_j \approx 5^\circ$), we consider the probabilities derived with this approach conservative.

5 Inferences on the Broadband Spectrum at 1234 days

The broadband X-ray-to-radio non-thermal emission from the jet afterglow of GW170817 at $\delta t < 900$ days is well fitted by a simple power-law spectral model $F_\nu \propto \nu^{-\beta}$ with $\beta = 0.583 \pm 0.013$,[22] or equivalently, $F_\nu \propto \nu^{-(p-1)/2}$ with $p = 2.166 \pm 0.026$ in the optically thin synchrotron regime. In this section we compute the constraints on the spectral slope at ~ 1234 days that are imposed by the X-ray detection (§1) and the 3 GHz radio limits (§2) under the assumption that the broadband spectrum is still described by a simple power-law model. Radio limits at 15 GHz and 0.8 GHz (§2-3), and HST observations[86] do not provide additional constraints on the simple power-law model (Extended Data Figure 4). We proceeded as follows. We used MCMC sampling within *Xspec* as described in §1 and we sampled 10^6 times the posterior probability distribution of the unabsorbed 0.3 – 10 keV flux derived from fitting the *CXO* data at $\sim$ 1234 days employing Cash-statistics. This method accounts for deviations from Gaussian statistics that manifest in the regime of low

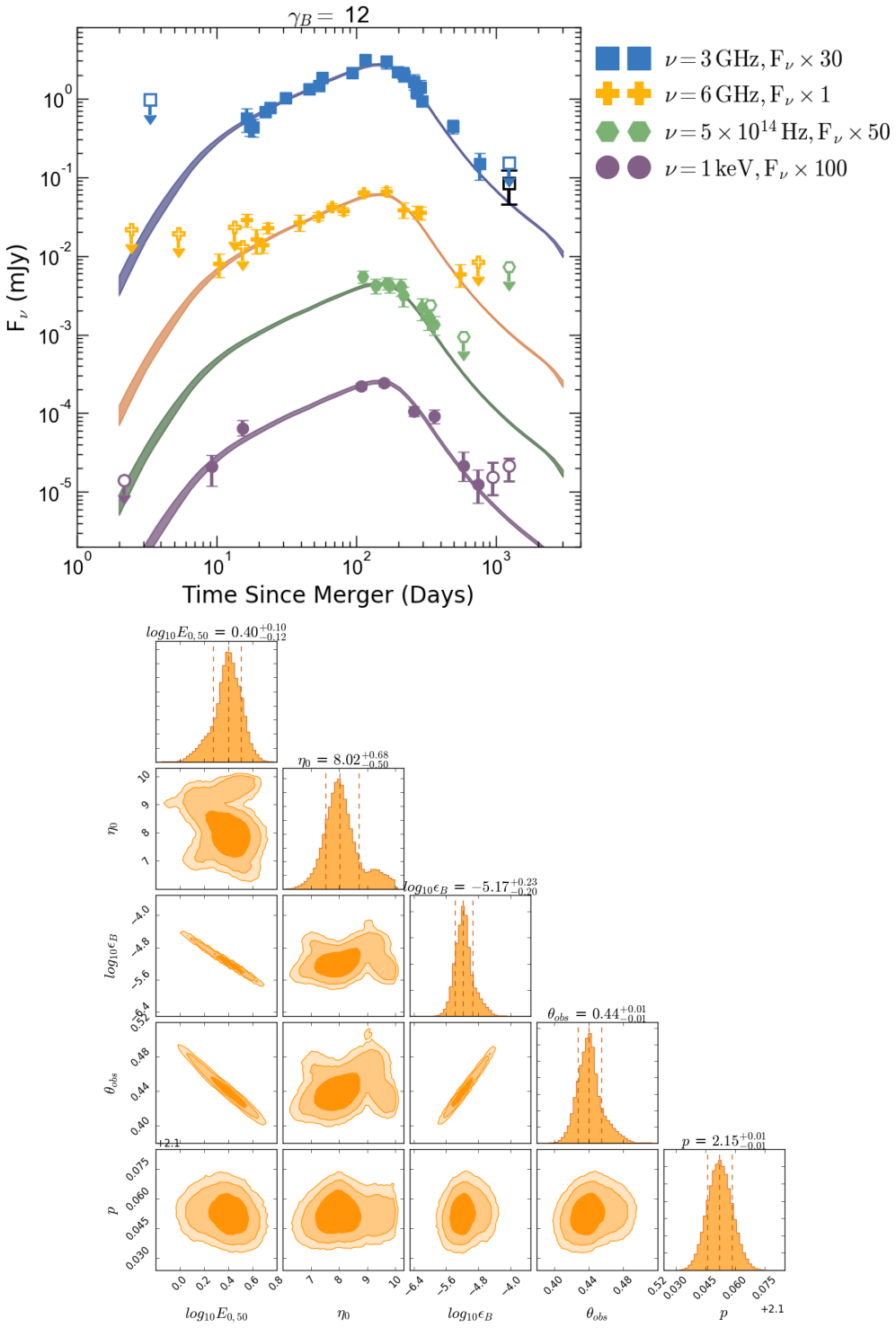

Extended Data Figure 2 | Broadband afterglow modeled by `JetFit` with $\gamma_B = 12$: *Top Panel:* Non-thermal emission from GW170817 across the electromagnetic spectrum and best fitting jet-afterglow model computed with `JetFit` for $n = 0.01\,cm^{-3}$, $\epsilon_e = 0.1$, and $\gamma_B = 12$. Empty symbols have not been included in the fitting procedure. Colored bands identify the 68% flux confidence interval. Black empty square symbol is the peak pixel value within one synthesized beam at the location of GW170817 at 3 GHz from Balasubramanian et al.[26]. *Bottom Panel:* One- and two-dimensional projections of the posterior distributions of the model's free parameters. Vertical dashed lines mark the 16^{th}, 50^{th}, and 84^{th} percentiles of the marginalized distributions (i.e. the median and 1-σ range). The contours are drawn at 68%, 95%, and 99% credible levels.

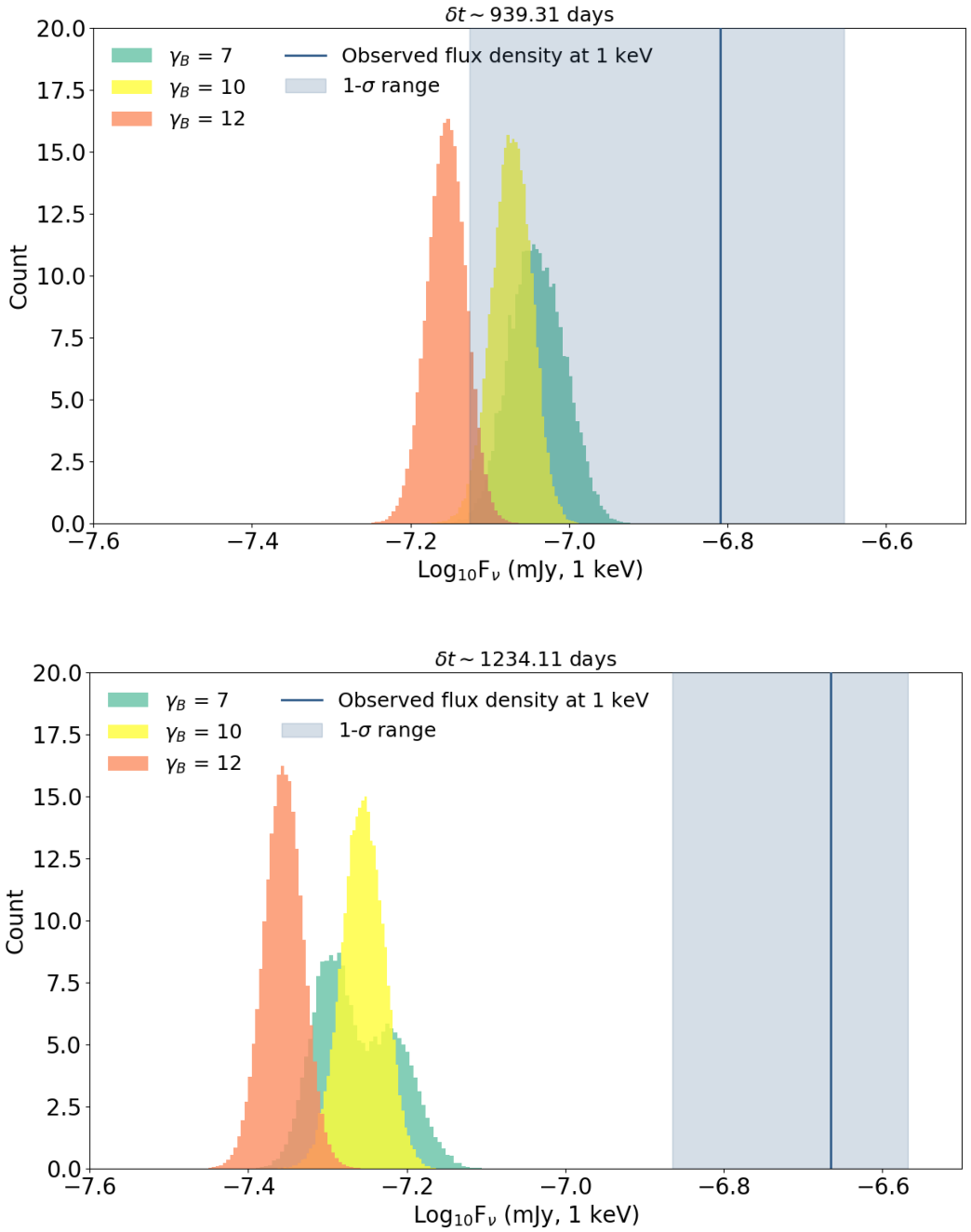

Extended Data Figure 3 | `JetFit` model flux distributions: *Top Panel:* Expected 1-keV flux density distributions at 939.31 days (histograms in color) derived from the fitting of the multi-wavelength afterglow of GW170817 in the time range $2 < \delta t < 900$ days using the code `JetFit`(using different values of γ_B). Vertical blue thick line and shaded area: observed X-ray flux density at this epoch and $\pm 1\sigma$ confidence range. *Bottom Panel:* Same as the top panel for 1234.11 days since merger.

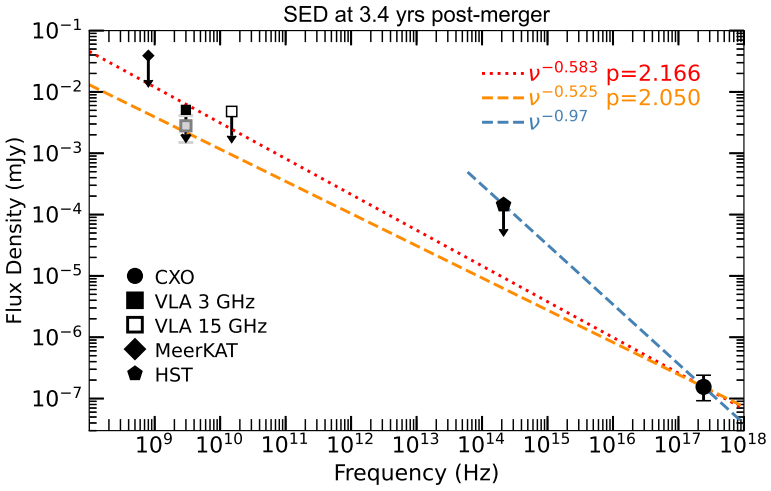

Extended Data Figure 4 | Broadband SED at 1234 days: Broad-band spectral energy distribution acquired around δt ≈3.4 years post-merger, including CXO X-ray data (filled circle), VLA upper limits at 3 and 15 GHz (filled and open square, respectively), MeerKAT flux limit (filled diamond) and HST/F140W flux limit (filled hexagon). Grey filled square: 3 GHz peak flux pixel value of $2.8\,\mu$Jy (with RMS of $1.3\,\mu$Jy) within one synthesized beam at the location of GW170817 from Balasubramanian et al.[26]. Red dotted line: $F_\nu \propto \nu^{-(p-1)/2}$ spectrum with $p = 2.166$ that best fitted the jet-afterglow data.[22] The VLA 3 GHz limit suggests a shallower spectrum (§5). Orange dashed line: $F_\nu \propto \nu^{-(p-1)/2}$ with $p = 2.05$. HST observations imply a NIR-to-X-ray spectral slope steeper than ≈ 1.

spectral counts. We then computed as a function of p the probability associated with spectral models $F_\nu \propto \nu^{-(p-1)/2}$ that would not lead to a radio detection, here defined as a 3 GHz radio flux density above 3, and 2 times the flux density root mean square – RMS – of our image around the location of GW170817, where RMS $= 1.7\,\mu Jy$.

Our results are shown in Extended Data Figure 5. We find that values of $p \geq 2.166$, i.e. larger than the best fitting value of the jet-afterglow at $\delta t < 900$ days are ruled out with statistical confidence $\geq 92\% - 99.2\%$. These results suggest the evolution of the broadband spectrum towards lower values of p and constitute the first indication of spectral evolution of the non-thermal emission from GW170817. This conclusion is strengthened by using the RMS $= 1.3\,\mu$Jy at 3 GHz from Balasubramanian et al.[26]

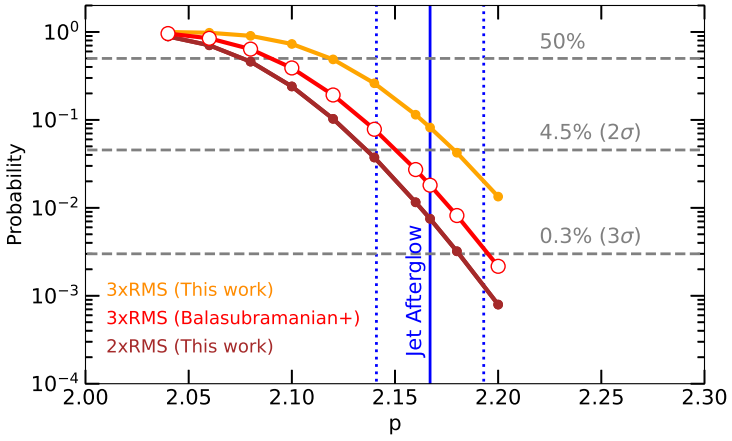

Extended Data Figure 5 | Probability of broadband spectral hardening: Probability of simple power-law $F_\nu = Norm \times \nu^{-(p-1)/2}$ spectral models at 1234 days that do not violate the 3×RMS (orange), and 2×RMS (brown) flux density of our 3 GHz image at the location of GW170817 as a function of p, where RMS=1.7 μJy. Red line and open symbols: results for RMS=1.3 μJy inferred by Balasubramanian et al.,[26] $Norm$ is drawn from the posterior probability distribution of the 0.3 – 10 keV unabsorbed X-ray flux at 1234 days as derived from MCMC sampling within *Xspec*. Horizontal grey dashed lines mark the 0.3%, 4.5% and 50% probability levels. Vertical blue thick and dotted lines: best fitting p parameter and $1\,\sigma$ range for the jet afterglow as derived from broadband SED fitting of the non-thermal emission of GW170817 at $\delta t < 900$ days.[22] This analysis suggests a hardening of the non-thermal spectrum of GW170817 at 1234 days to values of $p \leq$ than the best-fitting value from the earlier jet afterglow at statistical confidence $\geq 92\% - 99.2\%$.

We end by noting that HST observations[86] acquired on δt =1236.5 days since merger at $\nu = 2.13 \times 10^{14}$ Hz imply an optical to X-ray spectral index $\beta_{\rm OX} \lesssim 0.97$ (where $F_\nu \propto \nu^{-\beta_{\rm OX}}$). Finally, our VLA observations at 15 GHz reach a similar depth as our 3 GHz observations and rule out an optically thick radio source with flux density $F_\nu \geq 0.06\,\mu$Jy at $\nu = 3$ GHz.

6 Late time evolution of the emission from off-axis jet afterglows

In the context of synchrotron emission from an ultra-relativistic off-axis jet, a post-peak late-time flattening of the light-curve can be the result of[30,87]: (i) the jet encounter with an over-density in the environment; (ii) energy injection; (iii) time-varying shock microphysical parameters $\epsilon_{\rm B}$ and $\epsilon_{\rm e}$; (iv) transition into the sub-relativistic phase; and (v) emergence of the counter-jet emission.

The universal post jet-break light-curve evolution for an observed frequency ν above the synchrotron self-absorption frequency $\nu_{\rm sa}$ and for $\nu_m < \nu < \nu_c$ (where $\nu_{\rm m}$ is the synchrotron frequency and ν_c is the cooling frequency) is:[30]

$$F_\nu(\nu, t) \propto \epsilon_{\rm e}^{p-1} \epsilon_{\rm B}^{\frac{p+1}{4}} n^{\frac{3-p}{12}} E_k^{\frac{p+3}{3}} t^{-p} \nu^{\frac{1-p}{2}} \quad (1)$$

where E_k is the jet energy and n is the circum-burst density. The observed X-ray emission at 1234 days is a factor ≈ 4 above the extrapolation of the off-axis jet afterglow models (Figure 2). Explaining this excess of emission as a result of an over-density in the environment would require an exceedingly steep density gradient with n increasing by a factor of $\sim (4)^{\frac{12}{3-p}} \approx 3 \times 10^8$ (Eq. 1) over $\Delta r/r \approx 1$ at $r \approx 1$ pc. The characteristic size of the bow-shock cavity inflated by a pulsar wind (*if* any of the NS progenitors of GW170817 was a pulsar) scales as $R_s \propto n_{\rm ext}^{-1/2}$, where $n_{\rm ext}$ external medium density probed by the wind.[88] R_s is expected to be smaller than the shock

radius at this time if the density probed by the jet $n = 10^{-4} - 10^{-2}\,\mathrm{cm}^{-3}$ is representative of the density in the evacuated region (as it is reasonable to expect $n_{\rm ext} > n$). We thus consider the jet encounter with the edge of the pulsar wind bubble unlikely to occur at the time of our monitoring. Additionally, for a density contrast $\sim 10^8$ the implied amount of mass at $r \approx 1$ pc within the jet angle is $\geq 10\,\mathrm{M}_\odot$. Deep HST observations of the host galaxy environment of GW170817 rule out the presence of a globular cluster (GC) at the location of BNS merger.[22,89–92] The gravitational potential well of a GC might otherwise provide a physical reason for an abrupt change in the external gas density on the scale probed by the afterglow. We thus do not consider the over-density scenario any further.

Following a similar line of reasoning, an excess of emission can be produced if the shock is refreshed by the deposition of new energy.[94] From Eq. 1, a flux ratio of ≈ 4 requires the late-time deposition of a large amount of additional energy similar to the jet energy E_k. There is no natural energy source that can power the sudden energy release of an amount of energy equivalent to the jet energy at late times and we consider this scenario unlikely. Finally, a sharp variation of the shock microphysical parameters $\epsilon_{\rm e}$ and $\epsilon_{\rm B}$ with time can in principle lead to larger fluxes. This scenario would require an ad hoc evolution of $\epsilon_{\rm e}$ and $\epsilon_{\rm B}$ to explain the X-ray observations and we thus consider this model not physically motivated. Additionally, the deceleration of the shock is expected to lead to smaller ϵ_e values, while larger ϵ_e values would be needed to explain a flatter light-curve. In addition to the arguments above, we end by noting that all the models discussed so far do not naturally explain the harder radio-to-X-ray spectrum with a smaller value of p of §5.

In the absence of energy injection, environment over-densities and variations in the shock mi-

crophysical parameters, the transition of the blast wave dynamics to the sub-relativistic phase[28] at $t_{\rm NR} \approx 1100 (E_{\rm k,iso,53}/n)^{1/3}$ days is expected to lead to a smooth transition to a less steeply decaying light-curve $F_\nu \propto t^{-3(p-1)/2+3/5}$ at $\nu_m < \nu < \nu_c$ (Equation 97[28]) or $F_\nu \propto t^{-3(p-1)/2+1/2}$ at $\nu > \nu_c$ (equation A20[27]). For $p = 2.05 - 2.15$ we expect the light-curve to decay as $F_\nu \propto t^{-1.2} - t^{-1.0}$ in the non-relativistic regime. For the jet-environment parameters of GW170817[4,19–21] the full transition to the non-relativistic regime and the appearance of the counter jet is expected at $t_{\rm NR} \geq 5000$ days, significantly later than our current epoch of observation, with the start of the "deep Newtonian phase" being at even later times. In the deep Newtonian phase[29] $F_\nu \propto t^{-3(1+p)/10}$ or $F_\nu \propto t^{-0.9}$ for $p = 2.05 - 2.15$. A smooth transition to the sub-relativistic regime, accompanied by a slower light-curve decay, might start to be noticeable at earlier epochs, and possibly now, as the jet-core bulk Lorentz factor is $\Gamma(t) \approx 4 (t/100\,{\rm days})^{-3/8} \approx 1.6$ at the current epoch (in the Blandford-McKee regime, no jet spreading) or $\Gamma(t) \propto t^{-1/2}$ leading to $\Gamma(t) \approx 1.1$ for exponential jet spreading.[95] These estimates are based on the inferred $\Gamma \approx 4$ at ≈ 100 days.[19] In both cases the light-curve evolution is expected to be achromatic and the emission is expected to become dimmer with time as $F_\nu \propto t^{-1}$ or steeper. No re-brightening can be explained within the non-relativistic jet transition scenario and no spectral evolution is expected unless we invoke an ad hoc temporal evolution of p from $p = 2.15$ to $p = 2.0$ in the time range $900 - 1200$ days (i.e. well before the full transition to the non-relativistic phase) as the shock decelerates. The theoretical predictions from the Fermi process of particle acceleration in shocks would support this trend of evolution, as they predict $p = 2$ at non-relativistic shock speeds[33–35] and $p \sim 2.22$ at ultra-relativistic velocities in the test particle limit.[85,96–98] However, here the challenge is represented by having a

shock where the index of the non-thermal electron distribution p changes with time as a result of the shock deceleration, without having a substantial drop in the electron acceleration efficiency $\epsilon_{\rm e}$ when compared to the earlier ultra-relativistic regime.[99]

Finally, the emergence of the counter-jet emission is expected to lead to a flatter light-curve at $\delta t > t_{\rm NR}$, or $\delta t > 5000$ days for the parameters of GW170817. We conclude that the late-time evolution of the off-axis jet emission does not naturally account for the brightness, spectrum and the rapid change of slope of the X-ray light-curve at $\delta t \sim 1200$ days.

7 Kilonova Afterglow Models and Numerical Relativity Simulations of BNS Mergers

NS merger simulations predict the ejection of neutron-rich and neutron-poor matter due to a variety of mechanisms operating over different timescales during and after the merger.[100] These mass outflows shock the circumbinary medium producing synchrotron radiation that peaks on the deceleration time scale $t_{\rm dec}$.[7] The direct implication is that heavier mass outflows like those associated with the kilonova ejecta will produce non-thermal emission that will peak later in time than the emission associated with the significantly faster but also significantly lighter jet. For the inferred kilonova ejecta properties[11–18] of GW170817 ($M_{\rm ej} \approx 0.06\,{\rm M}_{\odot}$, $n \approx 0.01 - 0.001\,{\rm cm}^{-3}$ and $\beta \approx 0.1$ – 0.3), $t_{\rm dec} \approx 10^4$ days.[7] However, the deceleration of the fastest-moving tail of these ejecta is expected to contribute to non-thermal emission on significantly shorter timescales of months to years after the merger[7,32,101–103] that are relevant now (while the bulk of slower-moving ejecta powered the UV/optical/IR kilonova at $\delta t < 70$ days).

This kilonova afterglow will appear as an excess of emission compared to the off-axis jet afterglow.

Being powered by a different shock and by a different electron population than the jet's forward shock, the synchrotron emission from the kilonova afterglow does not necessarily inherit the same microphysical parameters $\epsilon_{\rm e}$, $\epsilon_{\rm B}$, as well as the electron index p. In this respect, the lower p value indicated by our observations would be a natural outcome and would be consistent with the $p < 2.2$ theoretical expectation of shocks that are non-relativistic.[33–35]

The kilonova afterglow emission strongly depends on (and is a tracer of) the kinetic energy distribution of the fastest kilonova ejecta $E_{\rm KN}(\Gamma\beta)$. We first adopt an analytical parametrization of $E_{\rm KN}(\Gamma\beta)$ to explore the large parameter space of the kilonova afterglow parameters while being agnostic to the ejecta type (e.g. winds vs. dynamical etc.). In the second part we employ a set of numerical relativity simulations of BNS mergers to emphasize the dependency of the observed kilonova afterglow on intrinsic parameters of the NS binary, like the binary mass ratio or the NS EoS.

The potential early emergence of the kilonova afterglow a few years after the merger, at a time when the jet has yet to effectively become spherical (§6) implies that the kilonova shock is expanding into a medium that is mostly unperturbed and that effects related to the jet evacuating the circum-merger medium[103] are unlikely to play a major role.

Kilonova afterglow models from Kathirgamaraju+2019: We parameterized the kinetic energy distribution of the kilonova ejecta as a power-law in specific momentum[32] $\Gamma\beta$ for $\beta > \beta_0$: $E_{\rm KN} \propto (\Gamma\beta)^{-\alpha}$. This parameterization captures the properties of the high-velocity tail of all types of kilonova outflows, including dynamical ejecta and disk winds that might dominate the mass of

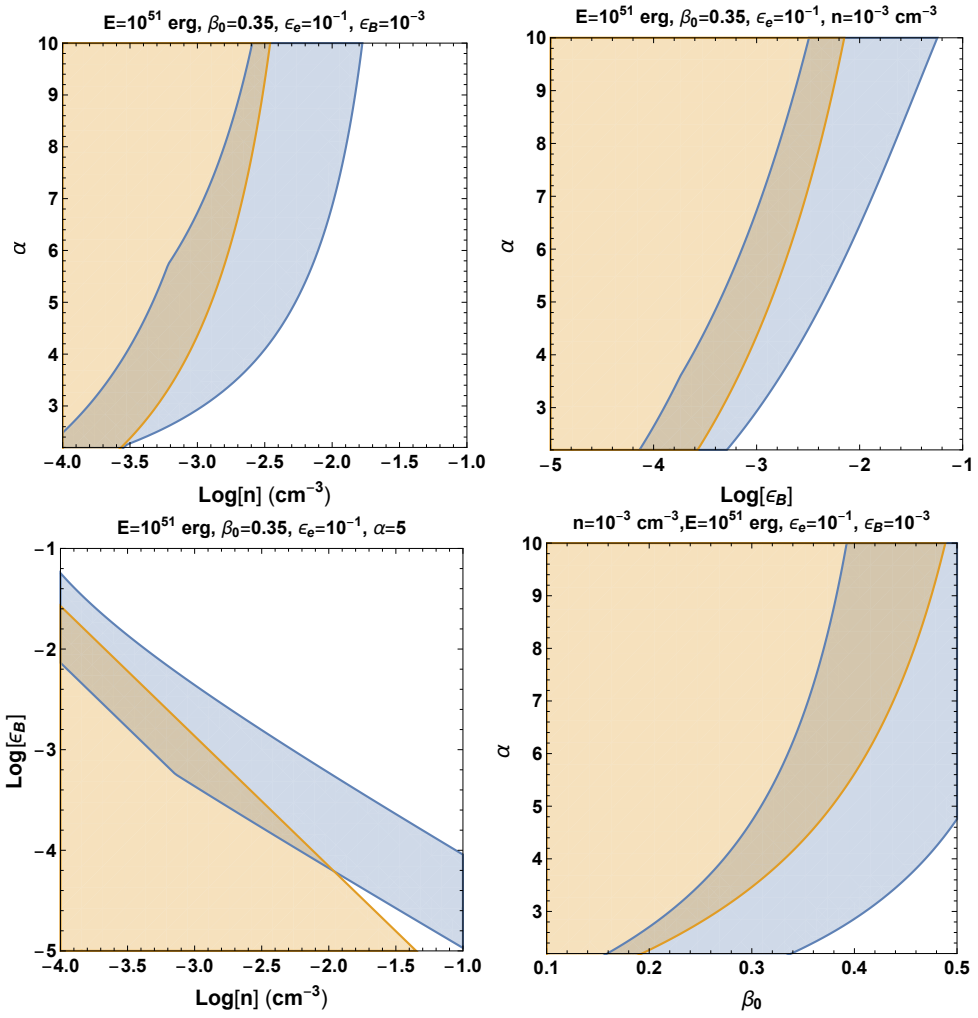

Extended Data Figure 6 | Constraints on the fastest moving kilonova ejecta: Blue shaded area: region of the parameter space consistent with the X-ray flux excess at 1234 days following the modeling described in §7. Orange shaded area: region of the parameter space that is consistent with our radio upper limit at 3 GHz: $F_\nu < 5.1\,\mu$Jy. The kinetic energy distribution of the kilonova ejecta in the velocity space has been parameterized as $E_{\rm KN} \propto (\Gamma\beta)^{-\alpha}$ above β_0 with $E_{\rm KN}(\Gamma_0\beta_0) = 10^{51}\,{\rm erg}$. The shock microphysical parameters adopted in this calculation are $p = 2.05$ (consistent with the observational findings of §5) and $\epsilon_{\rm e} = 0.1$. Two parameters are varied in each plot while the rest are kept fixed to values indicated in the plot title.

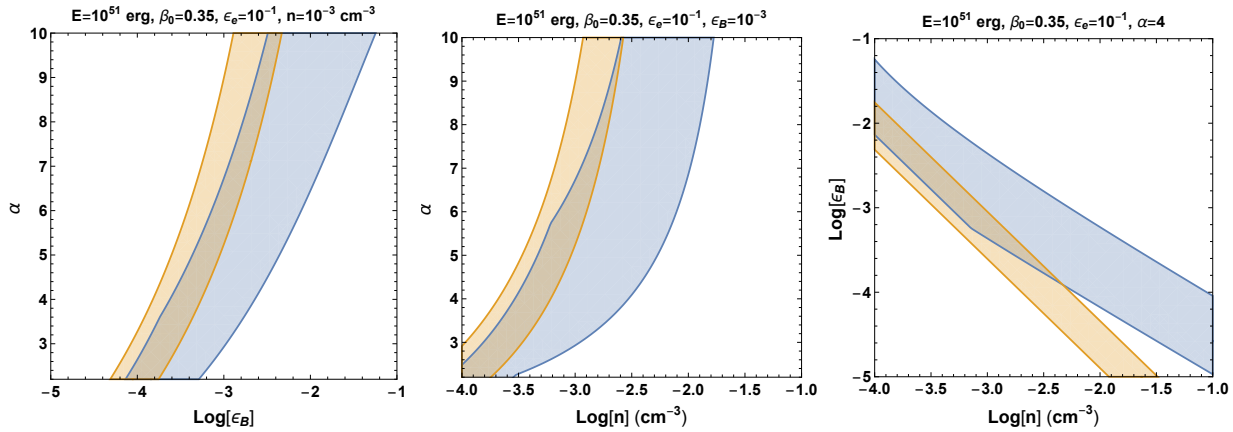

Extended Data Figure 7 | Kilonova constraints using 3 GHz flux density from Balasubramanian et al.: Kilonova afterglow parameter space with the same color scheme as Extended Data Figure 6 where we used the peak pixel flux within one synthesized beam at 3 GHz from Balasubramanian et al.,[26] ($F_\nu = 2.8 \pm 1.3\,\mu$Jy) as a constraint on the radio emission from the kilonova. Our conclusions remain unchanged.

the blue kilonova component. Motivated by the results from the modeling of the thermal emission from the kilonova[11–18] in the following we adopt $\beta_0 = 0.35$ as baseline and a total kinetic energy of $E_{\rm KN}(\Gamma_0\beta_0) = 10^{51}\,{\rm erg}$. We generated a set of multi-wavelength kilonova afterglow light-curves for shock microphysical parameters $p = 2.05$ (consistent with the observational findings of §5), $\epsilon_{\rm e} = 0.1$, $\epsilon_{\rm B} = [10^{-4}{-}10^{-2}]$ and circumbinary medium density $n = [10^{-4}{-}10^{-2}]\,{\rm cm}^{-3}$. As a comparison, studies of the jet afterglow pointed at densities[2] $n > 10^{-4}\,{\rm cm}^{-3}$, while studies[3,67,81] of the large-scale environment of GW170817 at X-ray and radio wavelengths led to $n \leq 10^{-2}\,{\rm cm}^{-3}$. Motivated by the results from numerical relativity simulations of BNS mergers described below we explore the parameter space for $\alpha = [3-9]$. Our results are shown in Extended Data Figure 6, where shaded areas highlight the regions of the parameter space that are consistent with the bright X-ray excess (blue) and the deep radio upper limit (orange). We further show a successful kilonova afterglow model for $\alpha = 5$, $n = 0.001\,{\rm cm}^{-3}$ and $\epsilon_{\rm B} = 0.001$ in Figure 2. Consistent with the results from the jet afterglow modeling, current data point at lower density environments with

$n < 0.01\,\mathrm{cm}^{-3}$, but otherwise leave the multi-dimensional parameter space largely unconstrained. Specifically, we find that all values of $\alpha = [3, 10]$ are consistent with the X-ray and radio data set. This conclusion remains unchanged even if we were to adopt the peak pixel flux within one synthesized beam at 3 GHz from Balasubramanian et al.,[26] ($F_\nu = 2.8 \pm 1.3\,\mu$Jy) as a constraint on the radio emission from the kilonova (Extended Data Figure 7).

Kilonova afterglows from physically-motivated kilonova kinetic energy profiles: We consider a set of 76 numerical relativity BNS merger simulations tailored to GW170817.[104–109] The simulations were performed using the `WhiskyTHC` code.[36–38] The set includes simulations performed at different resolutions and employs five finite-temperature microphysical equations of state (EoSs) that span the (large) range of EoS compatible with current laboratory and astronomical constraints. The simulations self-consistently included compositional and thermal effects due to neutrino emission and re-absorption.[110,111] The general-relativistic large-eddy simulation (GRLES) method was used to capture subgrid-scale turbulent dissipation and angular momentum transport.[112,113]

Dynamical ejecta from these simulations show the presence of a fast moving tail of ejecta, which is produced following the centrifugal bounce of the remnant taking place in the first milliseconds of the merger, unless prompt BH formation occurs, in which case there is no bounce.[111] The bounce produces a shock wave that is rapidly accelerated by the steep density gradient in the outer layers of the remnant and propels material to trans-relativistic velocities and propagates into the circumbinary medium. Fast moving material could also be accelerated by the thermalization of mass exchange flows between the stars prior to merger.[114] However, this alternative scenario typically predicts a faster rise of the synchrotron emission than what is indicated by observations

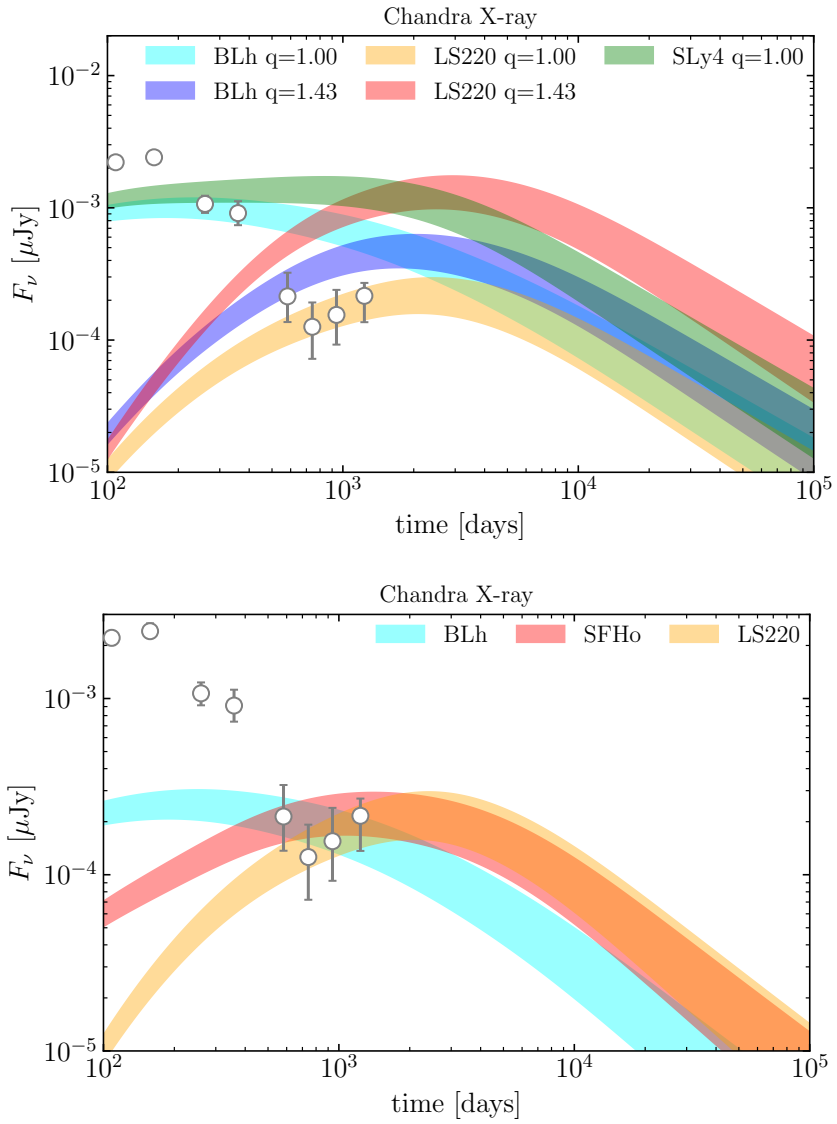

Extended Data Figure 8 | Kilonova afterglows from a set of ab-initio numerical relativity BNS merger simulations: *Upper Panel:* In these simulations the kilonova ejecta is of dynamical nature, with resulting kinetic energy profiles shown in Figure 3. Different colors correspond to different EoSs (BLh, LS220, and SLy4) and NS mass ratios q. Good quantitative agreement between the numerical relativity predictions and the observation is obtained. The light curves are computed assuming an ISM density of $n_{\rm ISM} = 6 \times 10^{-3}$ cm^{-3}, and microphysical parameters, $\epsilon_{\rm e} = 10^{-1}$, $\epsilon_{\rm B} = 10^{-2}$. *Lower Panel:* Effect of the extrinsic parameters (i.e. density and shock microphysics) on the kilonova afterglow emission from equal-mass NS binaries (i.e., $q \approx 1$ that is typical of the Galactic population) and different EoSs. For LS220, BLh and SFHo current observations are consistent with $n \sim 6 \times 10^{-3}, 5 \times 10^{-3}, 5 \times 10^{-3}\,{\rm cm}^{-3}$ and $\epsilon_{\rm B} \sim 10^{-2}, 2 \times 10^{-3}, 10^{-3}$, respectively, for a fiducial $\epsilon_{\rm e} = 0.1$. In both panels the viewing angle is assumed to be 30° from the polar axis. The bands correspond to light curves with the electron distribution power-law index p varying between 2.05 and 2.15.

of GW170817.

The deceleration of this kilonova shock into the medium produces synchrotron radiation. We compute the kilonova synchrotron light curves using the semi-analytic code `PyBlastAfterglow` (Nedora et al. in prep). We have validated this code in the subrelativistic regime by comparing the results it produces using the ejecta profiles from Radice et al. (2018)[111], which had been previously analyzed using the code of Hotokezaka & Piran (2015),[101] and in the ultrarelativistic regime by comparing our results with those produced by `afterglowpy`.[4]

Extended Data Figure 8 collects a representative set of X-ray light curves for three EoSs (BLh[106,115]; LS220[116]; and SLy4[117,118]) and two values of the binary mass ratio q. This figure highlights the sensitivity of the kilonova afterglow on intrinsic (EoS, q) and extrinsic (n, p, $\epsilon_{\rm e}$, $\epsilon_{\rm B}$) parameters of the binary. It is important to emphasize that the overall flux level predicted by our models is strongly dependent on assumed microphysical parameters of the shock. However, the light curve temporal evolution only depends on the structure of the ejecta and on the ISM density. Specifically, the peak time of the kilonova emission is of dynamical nature, traces the deceleration time of the blast wave into the environment[7] and it is thus independent from the parameters that set the level of the emitted flux (like the shock microphysical parameters).

With respect to the intrinsic binary parameters probed by our simulation, we find that binaries which do *not* undergo prompt BH formation are broadly consistent with the observations. An important conclusion from our study is that prompt BH formation is tentatively excluded,[45,119,120] because the presence of the post-merger bounce appears to be necessary in order to produce suf-

ficient fast and massive outflows to power the kilonova emission. Improved higher-resolution targeted simulations are needed to draw more quantitative conclusions.

We conclude by remarking that a general, robust and testable prediction of the kilonova afterglow models is that of a persistent source of emission across the electromagnetic spectrum, which is not expected to become fainter for thousands of days, and might even become brighter during this period of time. Eventually, the kilonova afterglow will appear as a detectable source in the radio sky and might even be detectable via deep optical observations from space.

8 Emission from a Compact-Object Remnant

An alternative explanation of rising X-rays without accompanying bright radio emission is that of central-engine powered radiation, i.e. radiation powered by an energy release associated with the compact-object remnant either in the form of accretion (for a BH remnant) or spin-down energy (for a long-lived NS remnant). The nature of the compact-object remnant of GW170817 is a fundamentally open question that directly relates to the NS EoS. While post-merger GWs were inconclusive, the observational evidence for (i) a blue kilonova component associated with a large mass of lanthanide-free ejecta and kinetic energy $\approx 10^{51}\,\mathrm{erg}$,[11,12,17,18,121] and (ii) the uncontroversial evidence for a successful relativistic jet,[19,20,58] together with energetics arguments strongly disfavor a prompt collapse to a BH and a long-lived NS remnant. These arguments and observations argue in favor of a hypermassive NS that collapsed to a BH within a second or so after the merger.[44–51] While the most likely scenario is that of a BH remnant at the current time of the observations, in the following we also consider the less-likely case of a spinning-down NS for

completeness.

Accreting BH scenario: The Eddington luminosity for accretion onto a remnant BH of mass[122] $M_\bullet \sim 2.5 M_\odot$ of GW170817 is given by

$$L_{\rm Edd} = \frac{4\pi G M_\bullet c}{\kappa_{\rm es}} \approx 8 \times 10^{38} \left(\frac{M_\bullet}{2.5 M_\odot}\right) \, {\rm erg \, s^{-1}}, \tag{2}$$

where $\kappa_{\rm es} = Y_e \sigma_{\rm T}/m_p \approx 0.16$ cm^2 g^{-1} is the approximate electron scattering opacity for fully ionized matter comprised of heavy elements (electron fraction $Y_e \simeq 0.4$).

From hydrodynamical simulations of BNS mergers,[123] the rate of fall-back accretion is $\dot{M}|_{t_0} \sim 2 \times 10^{-4} M_\odot$ s^{-1} on a timescale of $t_0 \sim 1$ s after the merger. A more important source of fall-back material may arise from the accretion disk outflows,[124] which likely dominated the kilonova ejecta in GW170817.[125] If a few tens of percent of the total ejecta mass $\approx 0.06 M_\odot$ inferred for GW170817[11,12,15,16,18] were to fall back to the BH on a timescale comparable to the predicted accretion disk lifetime ~ 1 s, the mass fall-back rate would be orders of magnitude higher, $\dot{M}|_{\rm t_0} \sim 10^{-2} M_\odot$ s^{-1}.

Based on the expectation that $\dot{M} \simeq \dot{M}_{t_{\rm fb}} (t/t_0)^{-5/3}$ at times $t \gg t_0$ for marginally bound material,[126] the total X-ray accretion luminosity is given by

$$\begin{aligned} L_{\rm X} \approx & \frac{\eta}{f_{\rm b}} \dot{M} c^2 \approx 10^{39} \left(\frac{f_{\rm b}}{0.1}\right)^{-1} \times \\ & \left(\frac{\eta}{0.1}\right) \left(\frac{\dot{M}|_{t_0}}{10^{-2} M_\odot \, {\rm s^{-1}}}\right) \left(\frac{t}{1000 \, {\rm days}}\right)^{-5/3} {\rm erg \, s^{-1}} \end{aligned} \tag{3}$$

where the radiative efficiency η has been normalized to that of a thin disk orbiting a BH of dimensionless spin[127] $a \approx 0.6 - 0.8$, as expected for the remnant of a BNS merger. Here $f_{\rm b}$ is the

geometric beaming fraction of the X-ray emission. We expect $f_{\rm b} \ll 1$ for sources at or near the Eddington luminosity (e.g., Ultraluminous X-ray sources, ULXs[128]) due to powerful disk outflows that generate a narrow accretion funnel.[129] We have normalized $f_{\rm b}$ to a lower limit based on the observer's viewing angle[19–21] $\theta_{\rm obs} \approx 0.4$ with respective to the original binary axis ($\simeq$ accretion disk angular momentum axis): $f_{\rm b,min} \approx \theta_{\rm obs}^2/2 \sim 0.1$.

In analogy with X-ray binaries in the "ultra luminous" state,[53] the spectra of stellar mass BHs accreting close to the Eddington rate are modeled well by a thermal disk with a power-law, and a break at higher energies. Ignoring relativistic terms and color corrections, the effective temperature of the disk emission can be estimated as

$$2\pi R_{\rm isco}^2 \sigma T_{\rm eff}^4 = f_{\rm b} L_{\rm X}, \tag{4}$$

where $R_{\rm isco} \approx 3GM_\bullet/c^2$ is the innermost radius of the disk for a BH of spin $a \approx 0.6 - 0.8$. This gives

$$kT_{\rm eff} \simeq 2\,{\rm keV} \left(\frac{f_{\rm b}}{0.1}\right)^{1/4} \left(\frac{L_{\rm X}}{5\times10^{38}{\rm erg\,s^{-1}}}\right)^{1/4} \left(\frac{M_\bullet}{2.5M_\odot}\right)^{-1/2}, \tag{5}$$

i.e. in the range of the *CXO* sensitivity window for the observed $L_{\rm X} \approx 5\times10^{38}{\rm erg\,s^{-1}}$ at 1243 days (Extended Data Table 1).

We now consider the question of the observability of this X-ray emission. The X-ray rise time will be determined by the maximum of two timescales. The first is the timescale for the accretion rate to drop sufficiently that the beaming fraction[129] $f_{\rm b} \propto (\dot{M}/\dot{M}_{\rm Edd})^{-2} \propto t^{10/3}$ increases to the point that the angle of the accretion funnel $\theta_{\rm b} \propto f_{\rm b}^{1/2} \propto t^{5/3}$ enters the observer's viewing angle $\theta_{\rm obs} \approx 0.4$. Given that $L_{\rm X}$ at the present epoch is $\lesssim L_{\rm Edd}$ (Eq. 2), we conclude that this effect may

still play a role in generating a rising X-ray luminosity.

A second timescale for the X-rays to be able to reach the observer is that required for the kilonova ejecta to become transparent to the X-rays. Assuming that the r-process ejecta have a bound-free opacity to photons of energy ~ 1 keV which is similar to that of iron group elements $\kappa_{\rm X} \approx 10^4$ cm^{-2} g^{-1}, this will take place after a time

$$t_{\rm thin} = \left(\frac{3M_{\rm ej}\kappa_{\rm X}}{4\pi v_{\rm ej}^2}\right)^{1/2} \approx 2000\,{\rm days}\left(\frac{v_{\rm ej}}{0.1{\rm c}}\right)^{-1}\left(\frac{\kappa_{\rm X}}{10^4\,{\rm cm^2\,g^{-1}}}\right)^{1/2}\left(\frac{M_{\rm ej}}{0.06M_\odot}\right)^{1/2}, \quad (6)$$

where we have normalized the ejecta mass $M_{\rm ej}$ and velocity $v_{\rm ej}$ to characteristic values for the (dominant) red/purple ejecta component inferred by modeling the optical/IR kilonova of GW170817.[11–14]

Given that the ejecta density may be lower than average for our high altitude viewing angle $\theta_{\rm obs} \approx 0.4$, and hence $t_{\rm thin}$ somewhat over-estimated, we conclude that $t_{\rm thin}$ is also likely to be comparable to the present epoch. An absorption cause for the X-ray rise could in principle be tested by a strong suppression of soft X-ray photons due to the rapidly increasing bound-free opacity towards lower-energy X-rays. However, due to faintness of the X-ray source (which leads to very low-count statistics, §1) combined with the progressive loss of sensitivity of the *CXO* at soft X-ray energies, this effect cannot be tested at present with any statistically meaningful confidence.

One potential constraint on this scenario comes from earlier IR/optical observations, since at earlier epochs the absorbed X-rays would be reprocessed to IR/optical radiation. For instance, to explain $L_{\rm x} \sim 5 \times 10^{38}$ erg s^{-1} at $t_{\rm now} \sim 10^3$ days, the accretion power on a timescale of $t_{\rm KN} \sim 1$ week after the merger would be higher by a factor $\sim (t_{\rm now}/t_{\rm KN})^{5/3} \approx 4000$, or $\sim 2 \times 10^{42}$

erg s^{-1}. The bolometric UV/optical/IR emission[12,15,16] from the kilonova of GW170817 reached $L \approx 10^{41}\,{\rm erg\,s^{-1}}$. The accretion power would thus exceed the bolometric output of the kilonova on this timescale by a factor $\gtrsim 10$. Even more stringently, extrapolating back to the last HST optical detection of GW170817 at ~ 360 days since merger leads to values $\approx 10^2$ times larger than the observed HST luminosity. At 360 days the optical flux density inferred from HST observations is perfectly consistent with the power-law spectrum that extends from the radio band to the X-rays,[22] and it is thus dominated by jet-afterglow emission.

However, there are two effects that act to alleviate these constraints. Firstly, at these earlier epochs the fall-back rate is highly super-Eddington. The efficiency with which the fall-back material reaches the central black hole may be drastically reduced at these early times due to the inability of the super-Eddington accretion to radiatively cool.[130] Furthermore, the radiative efficiency η of highly super-Eddington accretion flows may be substantially reduced relative to the near or sub-Eddington accretion rate which characterizes the present epoch. Finally, it is unclear if most of the reprocessed power will emerge in the optical/NIR bands; if lanthanide atoms dominate the cooling of the gas in the nebular phase then much of the reprocessed emission may emerge in the mid-IR bands.[131] On the other hand, *Spitzer* observations[132,133] revealed the 4.5μm luminosity to be $\sim 10^{38}$ erg s^{-1} on a timescale ≈ 74 days after the merger, at which time the fall-back accretion rate would be a factor ~ 100 higher than at present epoch. Thus we conclude that the reprocessing into the IR band is not a viable option, and would have to rely instead on the reduced accretion efficiency of the fall-back material onto the BH.

We end by commenting on the expected broadband spectrum. As GW170817 is accreting at or

close to the Eddington limit, it is valuable to contrast its observational properties with those of the ultra-luminous X-ray sources (ULXs), which accrete at or above the Eddington limit for compact objects at $\sim 1\,M_{\odot}$. Radio observations of ULX sources[54] place upper limits on the radio power of $\lesssim 10^{24}$ erg s^{-1} Hz^{-1}, corresponding to a flux density limit of $\lesssim 1\,\mu$Jy at the distance of GW170817, which is below the level of our latest radio upper limit of $\approx 5\,\mu$Jy (3$\times$RMS, §2) and interestingly comparable to the local image RMS in our deep VLA observations at 3 GHz. The lack of a radio counterpart of GW170817 is consistent with observations of XRBs in the "soft" state, which can accrete at a significant fraction of the Eddington rate and have no associated persistent radio emission.[52] Similarly, if GW170817 is accreting in a "hard" state (associated with an X-ray spectrum peaking at higher energies compared to the soft state), where the X-ray and radio emission are strongly coupled, [134] we would only expect a radio flux density of $\sim 10^{22}\,\mathrm{erg\,s^{-1}\,Hz^{-1}}$ based on our measured Chandra luminosity and the radio X-ray correlation[135] derived from an ensemble of 24 X-ray binaries in the hard state. Typically, X-ray binaries are only in the hard state while in quiescence (accreting at some small fraction of the Eddington rate) or while in outburst where they typically make the hard to soft state transition[136] at around $\sim 0.01\,L_{\rm Edd}$ to $\sim 0.1\,L_{\rm Edd}$. However, high luminosity hard states have been observed in the XRB GRS 1915+105,[137,138] but the associated radio emission would still be well below our detection threshold. We conclude by emphasizing that a solid expectation from this scenario is that of a different radio-to-X-ray spectrum than the jet afterglow, with less luminous radio emission than expected based on the jet-afterglow spectral slope. This is consistent with our observational findings (§5). Differently from the kilonova afterglow (§7, Extended Data Figure 8), in the BH fall-back accretion scenario the

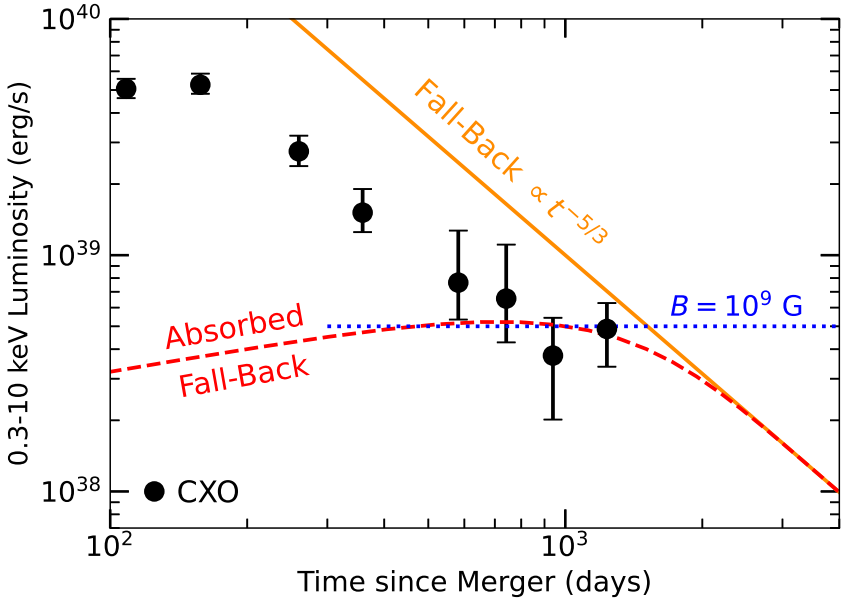

Extended Data Figure 9 | Emission from a compact-object remnant: Observed $0.3 - 10$ keV X-ray luminosity (black filled circles) compared to two sources of energy to power the X-ray excess in the compact-object powered scenario: (1) accretion-powered fall-back luminosity, both intrinsic (orange solid line) and observed (red dashed line), i.e. with a correction for absorption by the kilonova ejecta of the form $\propto (1 - e^{-(t/t_{\rm thin})^2})$, where $t_{\rm thin} \approx 1000$ days (Eq. 6). The dotted blue line shows the magnetar spin-down luminosity (Eq. 10) for $B \sim 10^9$ G to match the level of the observed X-ray emission.

X-ray luminosity is expected to decrease (Extended Data Figure 9).

To conclude, an accretion-powered origin of the emerging component of emission is a potentially viable explanation and would naturally account for the broadband spectrum *if* the efficiency of the super-Eddington fall-back matter reaching the black hole is suppressed sufficiently to prevent the accretion luminosity from violating the observed kilonova luminosity at earlier times.

Magnetar spin-down scenario: Alternatively, the additional X-ray component could be powered by spin-down energy from a long-lived magnetar remnant.[64] While there are theoretical arguments against the long-lived magnetar remnant scenario[45] we consider this scenario here for complete-

ness.

The massive NS remnant created by a BNS merger will in general have more than sufficient angular momentum to be rotating near break-up.[139] A NS of mass $M_{\rm ns}$ rotating near its mass-shedding limit possesses a rotational energy

$$E_{\rm rot} = \frac{1}{2} I \Omega^2 \simeq 1 \times 10^{53} \left(\frac{I}{I_{\rm LS}}\right) \left(\frac{M_{\rm ns}}{2.5 M_\odot}\right)^{3/2} \left(\frac{P}{0.7 {\rm ms}}\right)^{-2} {\rm erg}, \tag{7}$$

where $P = 2\pi/\Omega$ is the rotational period and I is the NS moment of inertia, which we have normalized to an approximate value for a relatively wide class of nuclear equations of state[140] $I_{\rm LS} \approx 1.3 \times 10^{45} (M_{\rm ns}/1.4 M_\odot)^{3/2}$ g cm^2.

The spin-down luminosity $L_{\rm sd}$ of an aligned dipole rotator of surface field strength B with $I = I_{\rm LS}$ is[141]

$$L_{\rm sd} = 7 \times 10^{50} \, {\rm erg \, s^{-1}} \left(\frac{B}{10^{15} \, {\rm G}}\right)^2 \left(\frac{P_0}{0.7 \, {\rm ms}}\right)^{-4} \left(1 + \frac{t}{t_{\rm sd}}\right)^{-2} \tag{8}$$

where we have taken $R_{\rm ns} = 12 \, {\rm km}$ as the NS radius, and

$$t_{\rm sd} = \left. \frac{E_{\rm rot}}{L_{\rm sd}} \right|_{t=0} \simeq 150 \, {\rm s} \left(\frac{I}{I_{\rm LS}}\right) \left(\frac{B}{10^{15} \, {\rm G}}\right)^{-2} \left(\frac{P_0}{0.7 \, {\rm ms}}\right)^2 \tag{9}$$

is the characteristic spin-down time over which an order unity fraction of the rotational energy is removed, where P_0 is the initial spin-period and we have assumed a remnant mass of $M = 2.3 M_\odot$.

To match a flat or rising X-ray luminosity at $\delta t \sim 1243$ days, $t_{\rm sd}$ must exceed the current epoch (~ 1000 days). In this regime, from Eq. 8:

$$L_{\rm sd} \simeq 7 \times 10^{50} \, {\rm erg \, s^{-1}} \left(\frac{I}{I_{\rm LS}}\right) \left(\frac{B}{10^{15} \, {\rm G}}\right)^2 \left(\frac{P_0}{0.7 \, {\rm ms}}\right)^{-4} \tag{10}$$

Matching the observed excess X-ray luminosity $L_{\rm X} \sim 5 \times 10^{38}$ erg s^{-1} would require an extremely weak magnetic field, $B \sim 10^9$ G. While this value is in the range of B inferred for recycled pulsars, this magnetic field is much smaller than the field strength $\gtrsim 10^{16}$ G expected to be amplified inside the remnant during the merger processes.[142]

The calculations above do not include the effects related to gravitational-wave losses that have been proposed in the context of the long-lived NS remnant scenario to dominate the magnetar spin-down at early times to avoid violating the inferred kilonova energy. However, it would still require fine-tuning to match $L_{\rm sd}$ to the observed $L_{\rm X}$ for a more physical value of B. Furthermore, unlike the BH case (Eq. 5), there is no reason *a priori* to expect the magnetar emission to occur in the X-ray range.

Extended Data Table 1 | Results from the analysis of *CXO* Observations of GW170817: Observed and inferred properties of the X-ray counterpart of GW170817 as constrained by the spectral analysis of *CXO* data with model `tbabs*ztbabs*cflux(pow)` within *Xspec*. The net count-rate is computed for $1''$ region, using source and background counts from `ds9`. We adopted a Galactic neutral hydrogen column density in the direction of the transient of $NH_{\rm gal} = 0.0784 \times 10^{22}\,{\rm cm}^{-2}$ and no intrinsic absorption. The uncertainties on the X-ray spectral parameters (photon index Γ and unabsorbed $0.3-10$ keV flux) have been computed with MCMC sampling and are reported at the $1\,\sigma$ c.l.. Upper limits are reported at the $3\,\sigma$ c.l.

δt[1] (days)	Significance[2] (σ)	Exposure (ks)	Net count-rate[3] (10^{-4} cts/s) (0.5 – 8 keV)	Γ[4]	Unabsorbed Flux (10^{-15} erg cm^{-2} s^{-1}) (0.3 – 10 keV)	Luminosity[5] (10^{38} erg s^{-1}) (0.3 – 10 keV)
2.33[6]	–	24.60	< 1.2	1.4	< 1.9	< 3.75
9.19	> 8	49.41	2.36 ± 0.70	$0.78^{+0.67}_{-0.56}$	$6.80^{+2.82}_{-2.92}$	$13.5^{+5.59}_{-5.79}$
15.39	> 8	96.1	2.95 ± 0.56	$2.05^{+0.49}_{-0.33}$	$5.32^{+1.42}_{-0.99}$	$10.6^{+2.81}_{-1.97}$
108.39	> 8	98.83	13.5 ± 1.17	$1.58^{+016}_{-0.16}$	$25.6^{+2.49}_{-2.34}$	$50.8^{+4.93}_{-4.65}$
157.76	> 8	104.85	13.7 ± 1.14	$1.64^{+0.15}_{-0.18}$	$26.7^{+2.90}_{-2.33}$	$52.8^{+5.74}_{-4.63}$
259.67	> 8	96.78	6.85 ± 0.85	$1.47^{+0.23}_{-0.22}$	$13.9^{+2.13}_{-2.01}$	$27.6^{+4.22}_{-3.98}$
358.61	> 8	67.16	3.94 ± 0.77	$2.02^{+0.44}_{-0.34}$	$7.67^{+1.76}_{-1.46}$	$15.2^{+3.50}_{-2.89}$
581.82	> 8	98.76	1.44 ± 0.39	$1.19^{+0.89}_{-0.61}$	$3.88^{+1.97}_{-1.40}$	$7.68^{+3.90}_{-2.77}$
741.48	6.5	98.86	1.03 ± 0.34	$0.92^{+0.91}_{-0.77}$	$3.32^{+1.75}_{-1.42}$	$6.58^{+3.46}_{-2.81}$
939.31	5.4	96.60	0.75 ± 0.29	1.603	$1.81^{+0.79}_{-0.94}$	$3.59^{+1.57}_{-1.86}$
1234.11	7.2	189.06	0.77 ± 0.21	1.603	$2.47^{+0.62}_{-0.91}$	$4.89^{+1.23}_{-1.80}$

[1] Exposure-time weighted average time since merger of all the observations within an epoch. The obsIDs within each epoch are as follows: 9 days: 19294; 15 days: 18988, 20728; 108 days: 20860, 28061; 158 days: 20936, 20937, 20938, 20939, and 20945; 260d: 21080, and 21090; 359 days: 21371; 582 days: 21322, 22157, and 22158; 742 days: 21372, 22736, and 22737; 939 days: 21323, 23183, 23184, and 23185; and 1234 days: 22677, 24887, 24888, 24889,2 3870, 24923, and 24924.
[2] Gaussian equivalent.
[3] Inferred from `dmcopy` and energy filtering in channels 500-8000.
[4] Spectral photon index, where $F_\nu \propto \nu^{-\beta}$ and $\Gamma = \beta + 1$.
[5] Calculated using a distance of 40.7 Mpc.[9]
[6] From reference[59].

Extended Data Table 2 | Radio Observations Log: Time on source for the VLA observations was calculated using the CASA analysis utilities task `timeOnSource`.

Start Date UTC	δt (days)	Observatory	Program/Project	On Source Time (minutes)	Mean Frequency (GHz)	Frequency Range (GHz)
15th Dec. 2020	1216.08	VLA	SL0449	204.23	3	2-4
27th Dec. 2020	1228.02	VLA	SL0449	204.23	3	2-4
2nd Feb. 2021	1264.95	VLA	SM0329	204.27	3	2-4
10th Feb. 2021	1272.88	VLA	SM0329	164.40	15	12-18
3rd Jan. 2021	1234.66	MeerKAT	DDT-20201218-JB-01	434.40	0.816	0.544-1.088

56. Margutti, R. *et al.* The Electromagnetic Counterpart of the Binary Neutron Star Merger LIGO/Virgo GW170817. V. Rising X-Ray Emission from an Off-axis Jet. *Astrophys. J. Lett.* **848**, L20 (2017). 1710.05431.

57. Haggard, D. *et al.* A Deep Chandra X-ray Study of Neutron Star Coalescence GW170817. *Astrophys. J. Lett.* **848**, L25 (2017). 1710.05852.

58. Alexander, A. *et al.* A Decline in the X-ray through Radio Emission from GW170817 Continues to Support an Off-Axis Structured Jet. *Astrophys. J. Lett.* **863**, L18 (2018). 1805.02870.

59. Margutti, R. *et al.* The Binary Neutron Star event LIGO/VIRGO GW170817 a hundred and sixty days after merger: synchrotron emission across the electromagnetic spectrum. *Astrophys. J. Lett.* **856**, L18 (2018). 1801.03531.

60. Nynka, M. *et al.* Fading of the X-ray Afterglow of Neutron Star Merger GW170817/GRB170817A at 260 days. *Astrophys. J. Lett.* **862**, L19 (2018). 1805.04093.

61. Troja, E. *et al.* The outflow structure of GW170817 from late time broadband observations. *Mon. Not. R. Astron. Soc.* **478**, L18 (2018). 1801.06516.

62. Ruan, J. J. *et al.* Erratum: "Brightening X-Ray Emission from GW170817/GRB 170817A: Further Evidence for an Outflow". *Astrophys. J. Lett.* **859**, L16 (2018). 1712.02809.

63. Pooley, D. *et al.* . *Astrophys. J. Lett.* **859**, L23 (2018). 1712.03240.

64. Piro, L. *et al.* A long-lived neutron star merger remnant in GW170817: constraints and clues from X-ray observations. *Mon. Not. R. Astron. Soc.* **483**, 1912 (2019). 1810.04664.

65. Troja, E. *et al.* A year in the life of GW170817: the rise and fall of a structured jet from a binary neutron star merger. *Mon. Not. R. Astron. Soc.* **489**, 1919 (2019). 1808.06617.

66. Hajela, A. *et al.* X-Ray Emission from GW170817 2.5 years After the Merger. *RNAAS* **4**, 68 (2020). –.

67. Makhathini, S. *et al.* The Panchromatic Afterglow of GW170817: The full uniform dataset, modeling, comparison with previous results and implications. *Arxiv e-prints* **-**, - (2020). 2006.02382.

68. Fruscione, A. *et al.* CIAO: Chandra's data analysis system. *SPIE* **6270**, 62701V (2006). 2006.02382.

69. Kalberla, P. M. W. *et al.* The LeidenArgentineBonn (LAB) Survey of Galactic HI. Final data release of the combined LDS and IAR surveys with improved stray-radiation corrections. *Astron. & Astrophys.* **440**, 775 (2005). astro-ph/0504140.

70. McMullin, J. P., Waters, B., Schiebel, D., Young, W., and Golap, K. CASA Architecture and Applications. *Astronomical Data Analysis Software and Systems XVI* **376**, 127 (2007). –.

71. Offringa, A. R. *et al.* WSClean: an implementation of a fast, generic wide-field imager for radio astronomy. *Mon. Not. R. Astron. Soc.* **444**, 606 (2014). 1407.1943.

72. Offringa, A. R., and Smirnov, O. An optimized algorithm for multiscale wideband deconvolution of radio astronomical images. *Mon. Not. R. Astron. Soc.* **471**, 301 (2017). 1706.06786.

73. Heywood, I. oxkat: Semi-automated imaging of MeerKAT observations. ascl:2009.003 (2020). 2009.003.

74. Kenyon, J. S., Smirnov, O. M., Grobler, T. L., and Perkins, S. J. CUBICAL - fast radio interferometric calibration suite exploiting complex optimization. *Mon. Not. R. Astron. Soc.* **478**, 2399 (2018). 1805.03410.

75. Tasse, C. *et al.* Faceting for direction-dependent spectral deconvolution. *Astron. & Astrophys.* **611**, A87 (2018). 1712.02078.

76. Mohan, N. and Rafferty, D. PyBDSF: Python Blob Detection and Source Finder. ascl:1502.007 (2015). 1502.007.

77. Lamb, G. P. *et al.* Late-time evolution of afterglows from off-axis neutron star mergers. *Mon. Not. R. Astron. Soc.* **481**, 2581 (2018). 1806.03843.

78. Dobie, D. *et al.* A turnover in the radio light curve of GW170817. *Astrophys. J. Lett.* **858**, L15 (2018). 1803.06853.

79. Mooley, K. *et al.* A Strong Jet Signature in the Late-time Light Curve of GW170817. *Astrophys. J. Lett.* **868**, L11 (2018). 1810.12927.

80. Alexander, K. D. *et al.* The Electromagnetic Counterpart of the Binary Neutron Star Merger LIGO/VIRGO GW170817. VI. Radio Constraints on a Relativistic Jet and Predictions for Late-Time Emission from the Kilonova Ejecta. *Astrophys. J. Lett.* **848**, L21 (2017). 1710.05457.

81. Hallinan, G. *et al.* A Radio Counterpart to a Neutron Star Merger. *Science* **358**, 1579 (2017). 1710.05435.

82. Mooley, K. *et al.* A mildly relativistic wide-angle outflow in the neutron star merger GW170817. *Nature* **554**, 207 (2018). 1711.11573.

83. Foreman-Mackey, D. *et al.* emcee: The MCMC Hammer. *Pub. Astron. Soc. Pac.* **125**, 306 (2013). 1202.3665.

84. Ryan, G. *et al.* Gamma Ray Bursts Are Observed Off-Axis. *Astrophys. J.* **799**, 3 (2015). 1405.5516.

85. Sironi, L., Spitkovsky, A. & Arons, J. *et al.* The Maximum Energy of Accelerated Particles in Relativistic Collisionless Shocks. *Astrophys. J.* **771**, 54 (2013). 1301.5333.

86. Kilpatrick, C. D., et al., GW170817: HST observations at 3.4 years from merger. *GCN* **29263** , (2021).

87. Nakar, E. & Piran, T. Afterglow constraints on the viewing angle of binary neutron star mergers and determination of the Hubble constant. *Arxiv e-prints* **-**, - (2021). 2005.01754.

88. Ramirez-Ruiz, E., Andrews, J. J., & Schrøder, S. L. Did GW170817 Harbor a Pulsar?. *Astrophys. J. Lett.* **883**, L6 (2019). 1905.09179.

89. Blanchard, P. K. *et al.* The Electromagnetic Counterpart of the Binary Neutron Star Merger LIGO/Virgo GW170817. VII. Properties of the Host Galaxy and Constraints on the Merger Timescale. *Astrophys. J. Lett.* **848**, L22 (2017). 1710.05458.

90. Levan, A. J. *et al.* The Environment of the Binary Neutron Star Merger GW170817. *Astrophys. J. Lett.* **848**, L28 (2017). 1710.05444.

91. Pan, Y. C. *et al.* The Old Host-galaxy Environment of SSS17a, the First Electromagnetic Counterpart to a Gravitational-wave Source. *Astrophys. J. Lett.* **848**, L30 (2017). 1710.05439.

92. Lamb, G. P. *et al.* The Optical Afterglow of GW170817 at One Year Post-merger. *Astrophys. J. Lett.* **870**, L15 (2019). 1811.11491.

93. Margutti, R. *et al.* The prompt-afterglow connection in gamma-ray bursts: a comprehensive statistical analysis of Swift X-ray light curves. *Mon. Not. R. Astron. Soc.* **428**, 729 (2013). 1203.1059.

94. Laskar, T. *et al.* Energy injection in gamma-ray burst afterglows. *Astrophys. J.* **814**, 1 (2015). 1504.03702.

95. Rhoads, J. E. The Dynamics and Light Curves of Beamed Gamma-Ray Burst Afterglows. *Astrophys. J.* **525**, 737 (1999). astro-ph/9903399.

96. Kirk, J. G., Guthmann, A. W., Gallant, Y. A. & Achterberg, A. Particle Acceleration at Ultrarelativistic Shocks: An Eigenfunction Method. *Astrophys. J.* **542**, 235 (2000). astro-ph/0005222.

97. Achterberg, A., Gallant, Y. A., Kirk, J. G. & Guthmann, A. W. Particle acceleration by ultrarelativistic shocks: theory and simulations. *Mon. Not. R. Astron. Soc.* **328**, 393 (2001). astro-ph/0107530.

98. Keshet, U. & Waxman, E. Energy Spectrum of Particles Accelerated in Relativistic Collisionless Shocks. *Phys. Rev. Lett.* **94**, 111102 (2005). astro-ph/0408489.

99. Crumley, P., Caprioli, D., Markoff, S. & Spitkovsky, A. Kinetic simulations of mildly relativistic shocks - I. Particle acceleration in high Mach number shocks. *Mon. Not. R. Astron. Soc.* **485**, 5105 (2019). 1809.10809.

100. Shibata, M., & Hotokezaka, K. Merger and Mass Ejection of Neutron-Star Binaries. *Ann. Rev. Nucl. Part. Sci.* **69**, 41 (2019). 1908.02350.

101. Hotokezaka, K., & Piran, T. Mass ejection from neutron star mergers: different components and expected radio signals. *Mon. Not. R. Astron. Soc.* **450**, 1430 (2015). 1501.01986.

102. Hotokezaka, K., Kiuchi, K., Shibata, M., Nakar, E. & Piran, T. Synchrotron radiation from the fast tail of dynamical ejecta of neutron star mergers. *Astrophys. J.* **867**, 95 (2018). 1803.00599.

103. Margalit, B., & Piran, T. Shock within a shock: revisiting the radio flares of NS merger ejecta and gamma-ray burst-supernovae. *Mon. Not. R. Astron. Soc.* **495**, 4981 (2020). 2004.13028.

104. Perego, A., Bernuzzi, S., & Radice, D. Thermodynamics conditions of matter in neutron star mergers. *Eur. Phys. J. A* **55**, 124 (2019). 1903.07898

105. Endrizzi, A. *et al.* Thermodynamics conditions of matter in the neutrino decoupling region during neutron star mergers. *Eur. Phys. J. A* **56**, 15 (2020). 1908.04952

106. Bernuzzi, S. *et al.* Accretion-induced prompt black hole formation in asymmetric neutron star mergers, dynamical ejecta and kilonova signals. *Mon. Not. R. Astron. Soc.* **497**, 1488 (2020). 2003.06015

107. Nedora, V. *et al.* Spiral-wave wind for the blue kilonova. *Astrophys. J. Lett.* **886**, L30 (2019). 1907.04872

108. Nedora, V. *et al.* Numerical Relativity Simulations of the Neutron Star Merger GW170817: Long-Term Remnant Evolutions, Winds, Remnant Disks, and NuclEoSynthesis. *Astrophys. J.* **906**, 98 (2021). 2008.04333

109. Perego, A. *et al.* Production of very light elements in kilonovae. *ArXiv e-prints* **–**, – (2020). 2009.08988

110. Radice, D. *et al.* Dynamical Mass Ejection from Binary Neutron Star Mergers. *Mon. Not. R. Astron. Soc.* **460**, 3255 (2016). 1601.02426

111. Radice, D. *et al.* Binary Neutron Star Mergers: Mass Ejection, Electromagnetic Counterparts and NuclEoSynthesis. *Astrophys. J.* **869**, 130 (2018). 1809.11161

112. Radice, D. General-Relativistic Large-Eddy Simulations of Binary Neutron Star Mergers. *Astrophys. J.* **838**, L2 (2017). 1703.02046

113. Radice, D. Binary Neutron Star Merger Simulations with a Calibrated Turbulence Model. *Symmetry* **12**, 1249 (2020). 2005.09002

114. Radice, D. *et al.* Viscous-Dynamical Ejecta from Binary Neutron Star Merger. *Astrophys. J. Lett.* **869**, L35 (2018). 1809.11163

115. Logoteta, D., Perego, A., & Bombaci, I. Microscopic equation of state of hot nuclear matter for numerical relativity simulations. *Astron. & Astrophys.* **646**, A55 (2021). 2012.03599

116. Lattimer, J M., & Swesty, F. D. A Generalized equation of state for hot, dense matter. *Nucl. Phys. A* **535**, 331 (1991). --

117. Douchin, F. & Haensel, P. A unified equation of state of dense matter and neutron star structure. *Astron. & Astrophys.* **380**, 151 (2001). astro-ph/0111092

118. Schneider, A. S., Roberts, L. F., & Ott, C. D. Open-source nuclear equation of state framework based on the liquid-drop model with Skyrme interaction. *Phys. Rev. C.* **96**, 065802 (2017). --

119. Bauswein, A., Just, O., Janka, H., & Stergioulas, N. Neutron-star Radius Constraints from GW170817 and Future Detections. *Astrophys. J. Lett.* **850**, L34 (2017). 1710.06843

120. Radice, D., Perego, A., Zappa, F., & Bernuzzi, S. GW170817: Joint Constraint on the Neutron Star Equation of State from Multimessenger Observations. *Astrophys. J. Lett.* **852**, L29 (2018). 1711.03647

121. Evans, P. A. *et al.* Swift and NuSTAR observations of GW170817: Detection of a blue kilonova. *Science* **358**, 6370 (2017). 1710.05437.

122. Abbott, B. P. *et al.* Properties of the Binary Neutron Star Merger GW170817. *Phys. Rev. X* **9**, 011001 (2019). 1805.11579.

123. Rosswog, S. Fallback accretion in the aftermath of a compact binary merger. *Mon. Not. R. Astron. Soc.* **376**, L48 (2007). astro-ph/0611440.

124. Fernandez, R. & Metzger, B. D. Delayed outflows from black hole accretion tori following neutron star binary coalescence. *Mon. Not. R. Astron. Soc.* **435**, 502 (2013). 1304.6720.

125. Radice, D., Bernuzzi, S. & Perego, A. The Dynamics of Binary Neutron Star Mergers and GW170817. *Ann. Rev. Nucl. & Part. Sci.* **70**, 95 (2020). 2002.03863.

126. Rees, M. J. Tidal disruption of stars by black holes of 106-108 solar masses in nearby galaxies. *Nature* **333**, 523 (1988). –.

127. Novikov, I. D. & Thorne, K. S. Astrophysics of black holes. *Black Holes (Les Astres Occlus)*, 343 (1973). –.

128. Walton, D. J. *et al.* A Potential Cyclotron Resonant Scattering Feature in the Ultraluminous X-Ray Source Pulsar NGC 300 ULX1 Seen by NuSTAR and XMM-Newton *Astrophys. J. Lett.*, **857**, L3 (2018). 1803.07571.

129. King, A. R. Masses, beaming and Eddington ratios in ultraluminous X-ray sources. *Mon. Not. R. Astron. Soc.* **393**, L41 (2009). 0811.1473.

130. Rossi, E. M. & Begelman, M. C. Delayed X-ray emission from fallback in compact-object mergers *Mon. Not. R. Astron. Soc.* **392**, 1451 (2009). 0808.1284.

131. Hotokezaka, K. *et al.* Nebular Emission from Lanthanide-rich Ejecta of Neutron Star Merger *Arxiv e-prints* **-**, - (2021). 2102.07879.

132. Villar, V. A. *et al.* Spitzer Space Telescope Infrared Observations of the Binary Neutron Star Merger GW170817 *Astrophys. J. Lett.* **862**, L11 (2019). 1805.08192.

133. Kasliwal, M. M. *et al.* Spitzer Mid-Infrared Detections of Neutron Star Merger GW170817 Suggests Synthesis of the Heaviest Elements *Mon. Not. R. Astron. Soc.* **-**, L14 (2019). 1812.08708.

134. Corbel, S., Nowak, M. A., Fender, R. P., Tzioumis, A. K. & Markoff, S. Radio/X-ray correlation in the low/hard state of GX 339-4 *Astron. & Astrophys.* **400**, 1007 (2003). astro-ph/0301436.

135. Gallo, E. *et al.* The radio/X-ray domain of black hole X-ray binaries at the lowest radio luminosities *Mon. Not. R. Astron. Soc.* **445**, 290 (2014). 1408.3130.

136. Dunn, R. J. H., Fender, R. P., Körding, E. G., Belloni, T. & Cabanac, C. A global spectral study of black hole X-ray binaries *Mon. Not. R. Astron. Soc.* **403**, 61 (2010). 0912.0142.

137. Rushton, A., Spencer, R. E., Pooley, G. & Trushkin, S. A decade of high-resolution radio observations of GRS1915+105 *Mon. Not. R. Astron. Soc.* **401**, 2611 (2010). 0910.1779.

138. Motta, S. E *et al.* Observations of a radio-bright, X-ray obscured GRS 1915+105 *Mon. Not. R. Astron. Soc.* **503**, 152 (2021). 2101.01187.

139. Radice, D., Perego, A., Bernuzzi, S., & Zhang, B. Long-lived remnants from binary neutron star mergers *Mon. Not. R. Astron. Soc.* **481**, 3670 (2018). 1803.10865.

140. Lattimer, J. M., & Schutz, B. F. Constraining the Equation of State with Moment of Inertia Measurements *Astrophys. J.* **629**, 979 (2005). astro-ph/0411470.

141. Philippov, A. A., Spitkovsky, A. & Cerutti, B. Ab Initio Pulsar Magnetosphere: Three-dimensional Particle-in-cell Simulations of Oblique Pulsars *Astrophys. J. Lett.* **801**, L19 (2015). 1412.0673.

142. Kiuchi, K. *et al.* Efficient magnetic-field amplification due to the Kelvin-Helmholtz instability in binary neutron star mergers *Phys. Rev. D* **92**, 124034 (2015). 1509.09205.